

Cosmological consequences and statefinder diagnosis of a non-interacting generalized Chaplygin gas in $f(R, T)$ gravity

Hamid Shabani,*

Department of Physics, University of Sistan and Baluchestan,
Zahedan, Iran

November 1, 2016

Abstract

In this paper, we investigate cosmological consequences of a scenario for recently reported accelerated expansion of the Universe, in which the generalized Chaplygin gas (GCG) along with the baryonic matter are responsible for this observed phenomenon. In the present model, we employ an isotropic and homogeneous FLRW space time in the framework of $f(R, T)$ theory of gravity. In $f(R, T)$ gravity, the conservation of energy-momentum tensor (EMT) leads to a constraint equation which enforces us to use some specific forms of type $f(R, T) = g(R) + h(T)$. In this work we choose $g(R) = R$. We consider three classes of Chaplygin gas models which include three different forms of $f(R, T)$ function; those models which employ the standard Chaplygin gas (SCG), models which use GCG in the high pressure regimes and finally, the third case is devoted to investigating high density regimes in the presence of GCG. The effective equation of state (EoS) and the deceleration parameter for these Chaplygin gas models are calculated and it is indicated that the related present values can be observationally acceptable in $f(R, T)$ gravity. Among the models we shall present, type two models has a better situation; the predictions of these models are more consistent with the observational data. We also examine these models via the statefinder diagnostic tool. The statefinder parameters s and r are obtained for these three scenarios and various trajectories are plotted for different values of the model parameters. The involved parameters are, K and α which appear in the GCG density and the parameters \mathbf{m} and \mathbf{n} which are related to the integral constants which are appeared in the process of obtaining $h(T)$. The discrimination between different dark energy models is considered by varying the mentioned parameters for these three types of models. Since positive

*h.shabani@phys.usb.ac.ir

values for \mathbf{m} and \mathbf{n} 's would lead to some divergences, we will take negative values. It is discussed that the consistent values for the effective EoS for all allowed values of K , can only be obtained in the high pressure regimes. We show that the distance of these models (which is defined as the difference between the predicted present values of the statefinder parameters of a model and the corresponding ones for Λ CDM model), varies for different choices of the model parameters. However, the distance does not depend on the values of α for models of type three. Finally, we test these Chaplygin gas models using recent Hubble parameter as well as type Ia supernova data. We find that these models are compatible with type Ia supernova data. Particularly, we plot the modulus distance, the Hubble parameter and the effective EoS parameter for the best fit values of the model(s) parameters. Also, we compare the predicted present values of the statefinder parameters to the observational data.

1 Introduction

Currently, observational experiments show that the Universe is undergoing an accelerated expansion [1, 2, 3, 4, 5, 6, 7, 8, 9, 10, 11]. The most accepted agreement is that there is two components which play a serious and important role in the formation and evolution of the Universe; the so called "dark matter" (DM), which is responsible for the structure formation and clustering of the galaxies [12, 13, 14, 15, 16, 17, 18, 19] and the "dark energy" (DE) which makes a negative pressure and thus gives rise to the accelerated expansion of the Universe [20, 21, 22, 23, 24, 25, 26, 27, 28, 29, 30, 31]. The former has a contribution of about 26% of the total matter density, the latter forms about 69% of it and the rest is related to the baryonic (visible) matter [32, 33]. There are two general approaches which can be used to face the problems associated to DE and DM. The first one deals with introducing some matter field(s) that affect the dynamical evolution of the universe and thereby these observed phenomena may be explained. In the second approach one can alter the geometrical sector of GR to obtain some theoretical results corresponding to the observational ones. In order to apply the former, numerous scenarios have been proposed so far. The cosmological constant can be accounted for as the most successful and important candidate for DE which has a constant EoS parameter. The GR theory comprised by the cosmological constant and DM is called the concordance or the Λ CDM model [34]. In spite of high consistency of Λ CDM model with the present observations, it suffers from an important problem; the theoretical value of the DE density is not compatible with the observationally accepted one. Indeed, their values differ about 120 orders of magnitude. This problem is called "the cosmological constant problem" [35, 36, 37, 38, 39, 40, 41, 42]. The other proposals for the accelerated expansion of the Universe are the dynamical DE models with time-varying EoS e.g., quintessence and phantom models [43, 44, 45, 46, 47, 48]. However, these models may also include other problems, e.g., the "fine tuning" which is a major issue, by which the quintessence models are afflicted. Another candidate for DE (which is the main subject of our study) is the Chaplygin gas

(CG) model introduced as to explain the DE phenomenon [49, 50]. Following a perfect fluid, the EoS for this matter is, $p = -K/\rho$ where K is a constant (this case is called the standard Chaplygin gas (SCG)). It has been shown that the Chaplygin cosmology can be interpreted as a transition from a DM dominated universe to an accelerated expansion universe including an intermediate phase with “stiff fluid” (which corresponds to a fluid with $p = \rho$) domination [51]. Although, the SCG model can lead to a transition from a decelerated to accelerated expansion, it cannot explain the structure formation and it is encountered some problems with the cosmological power spectrum [53, 54]. Consequently, the EoS of the SCG model has been generalized as $p = -K/\rho^{-\alpha}$, to confront the mentioned issues. Note that, the general CG model (GCG) gives rise to an intermediate epoch with the EoS $p = \alpha\rho$ [50]. The GCG model has been used in different areas such as, the DE problem [55, 56], Matter power spectrum [57] and wormholes [58, 59, 60].

The geometrical manipulation of GR is the other approach with the aim of solving some problems such as DE and DM. In the past decades, higher order gravity, specially $f(R)$ gravity has been introduced by replacing the Ricci scalar in the Einstein-Hilbert action with some scalar invariants. This model has drawn a remarkable attention among the other models and theories. In $f(R)$ theory of gravity, one simply replaces the Ricci curvature scalar with a function of it. This theory has had successes and failures in different aspects [61, 62, 63, 64, 65, 66, 67, 68, 69, 70]. As an idea toward the development of $f(R)$ gravity, some authors assume that the matter Lagrangian is non-minimally coupled to the geometrical sector of the action [71, 72, 73, 74, 75]. In Ref. [76] a more complete form of these type of models entitled as $f(R, L_m)$ gravity is proposed. Another suggestion to couple the matter sector to the geometrical one is to employ the trace of EMT. This model was presented by authors of Ref. [77], and various features of this model have been reported in [78, 79, 80, 81, 82, 83, 84, 85, 86, 87, 88, 89, 90, 91].

In the present work we use both approach, namely, we work on a model in which GCG and the baryonic matter are considered as the whole matter in $f(R, T)$ gravity as the background geometric law. Simultaneously use of both approach have been already employed in the literature to describe the early or late time phenomena in cosmology [101, 102]. Since $f(R, T)$ gravity introduces a new approach to involve the interactions of matter effects with spacetime curvature, it is well-motivated to consider cosmological consequences of different types of matter in the framework of this theory. The GCG in the background of GR involved some issues e.g., the standard case, namely SCG has ruled out by the most observational data or in some works it is reported that only specific subclasses of solutions would pass the observational tests (i.e., those with $\alpha \sim 0$) [95, 96, 97, 98, 99, 100]. Authors of Ref. [103] have shown that CG produces oscillations or exponential blowup of the power spectrum of dark matter which is not consistent with observations. Particularly, they have reported that 99.999% of GCG parameter space which previously has been allowed, would be excluded. However, in Ref. [104] it has been discussed that considering the joint effect of shear and rotation can overcome this instability. In this regard, the study of Chaplygin gas in other frameworks such as $f(R, T)$

gravity, in search of a viable dark energy model may leads to more desirable results. Cosmological considerations of every theory of gravity are based on the investigation of the behavior of the Hubble and the deceleration parameters which are defined as the first and second order of time derivatives of the scale factor i.e., $H = \dot{a}/a$, $q = \ddot{a}/(aH^2)$. The former determines the expansion of the Universe and the latter indicates the acceleration/deceleration behavior. The DE models are constructed so as to match them with the observations. For this reason, the most consistent DE models give the same present values of H and q . Therefore, there is some type of degeneracy in the present values, H_0 and q_0 . To deal with this issue, various strategies have been proposed. The statefinder diagnosis is an efficient tool to discriminate different DE models. The authors of Ref. [105] introduced new cosmological parameters constructed out of the third order of time derivative of the scale factor which are called "statefinder parameters" and are denoted by the pair $(s \equiv (r-1)/3(q-1/2), r \equiv \ddot{a}/(aH^3))$. Since, this tool use the different orders of the time derivative of the scale factor, it is a geometrical diagnosis. This method can distinguish between DE models that have the same values of H_0 and q_0 , in a higher level. Note that this method can be extended to the models with higher degrees of degeneracy. In the statefinder diagnostic tool, the DE models indicated by the (s, r) plane trajectories and in this way one could consider the behavior of different DE models and thus discriminate them. We have mentioned that the Λ CDM model is still good fitted to the observation and therefore the suggested DE models should not be so far from this model. To understand this fact, the difference between the predicted present values s_0 and r_0 of models and the corresponding values of Λ CDM model $(s_0^{(\Lambda\text{CDM})}, r_0^{(\Lambda\text{CDM})})$ is a criteria for distinction of the DE models (this difference is called "distance of model").

Up to now, different DE models are diagnosed which are mainly of scalar field type models, such as Λ CDM and quintessence DE models which have been considered in [105, 106] and are accounted for as the first research works that introduced the statefinder diagnostic tool, the interacting quintessence models [107, 108], the holographic DE models [109, 110], the holographic DE model in a non-flat universe [111], the phantom model [112], the tachyon model [113], the GCG model [114] and the interacting new agegraphic DE model in a flat and a non-flat universe [115, 116].

We plan our investigations as follows: in Sec. 2, we start with presenting the action of $f(R, T)$ gravity and obtain the related field equations and a constraint that must be satisfied by the function $f(R, T)$ in order to guarantee the conservation of EMT. We devote the rest of this section to present the procedure of obtaining the function $f(R, T)$. For some reasons we presume a linear combination of the matter and curvature sectors of the Lagrangian, i.e., $f(R, T) = R + h(T)$. This choice facilitates the procedure of obtaining $f(R, T)$ function using the EMT conservation and makes us capable of getting exact solutions. Minimal couplings respect the EMT conservation and for these type of models all equations and solutions can be easily reduced to GR. These models can be seen as a modification to GR. Also, the models including minimal

couplings respect the equivalence principle, in spite of non-minimal ones which show some violation, in this respect [117, 118]. We get three classes of $f(R, T)$ function. Class I for the SCG model, class II for the GCG model in high pressure situations and class III for the GCG model in high density regimes. In Sec. 3 we introduce the statefinder parameters and obtain them for these three models. Moreover, we bring forward some cosmological parameters that are helpful for the rest of our study. In Sec. 4, we present adequate numerical plots to show and discuss the cosmological consequences of these three models. Sec. 5 has been devoted to testing models I, II and III using the recent observational data via the chi-square technique and finally, in Sec. 6 we summarize our results.

2 Field equations of $f(R, T)$ gravity and the conservation of EMT

In this section we present the field equation of $f(R, T)$ theory of gravity and also discuss the conservation of EMT when two pressureless baryonic matter and GCG¹ are taken into account. By including the two forms of matters, the action of $f(R, T)$ theory of gravity can be written as

$$S = \int \sqrt{-g} d^4x \left[\frac{1}{16\pi G} f(R, T^{(b, G)}) + L^{(total)} \right], \quad (1)$$

where we have defined the Lagrangian of the total matter as

$$L^{(total)} \equiv L^{(b)} + L^{(G)}. \quad (2)$$

In the above equations R , $T^{(b, G)} \equiv g^{\mu\nu} T_{\mu\nu}^{(b, G)}$, $L^{(b, G)}$ are the Ricci curvature scalar, the trace of EMT of the baryonic matter and GCG (which we get these fluids as the total matter content of the Universe) and the Lagrangian of the total matter, respectively. The superscripts b and G stand for the baryonic matter and GCG, g is the determinant of the metric and we set $c = 1$. The EMT $T_{\mu\nu}^{(b, G)}$ is defined as the Euler-Lagrange expression of the Lagrangian of the total matter, i.e.,

$$T_{\mu\nu}^{(b, G)} \equiv -\frac{2}{\sqrt{-g}} \frac{\delta [\sqrt{-g}(L^{(b)} + L^{(G)})]}{\delta g^{\mu\nu}}. \quad (3)$$

Instead of obtaining the field equations for the action (1), it is sufficient to obtain the corresponding field equations of $f(R, T)$ gravity for general trace T and the matter Lagrangian $L^{(m)}$, and then solve them using the related quantities of the two forms of matters; namely, the baryonic matter and GCG.

¹As we shall discuss, GCG has a dual feature in the past and future. It behaves like the cold dark matter (CDM) in the early times and DE in the late times. Thus, we use GCG as it plays the role of dark sector of the Universe.

If in the action (1), the trace $T^{(\text{b}, \text{G})}$ and $L^{(\text{total})}$ are replaced by trace T and $L^{(\text{m})}$, respectively, the field equations for $f(R, T)$ gravity can be obtained as [77]

$$F(R, T)R_{\mu\nu} - \frac{1}{2}f(R, T)g_{\mu\nu} + \left(g_{\mu\nu}\square - \nabla_\mu\nabla_\nu\right)F(R, T) = \left(8\pi G - \mathcal{F}(R, T)\right)T_{\mu\nu} - \mathcal{F}(R, T)\Theta_{\mu\nu}, \quad (4)$$

where

$$\Theta_{\mu\nu} \equiv g^{\alpha\beta} \frac{\delta T_{\alpha\beta}}{\delta g^{\mu\nu}} \quad \text{and} \quad T_{\mu\nu} \equiv -\frac{2}{\sqrt{-g}} \frac{\delta\left(\sqrt{-g}L^{(\text{m})}\right)}{\delta g^{\mu\nu}}, \quad (5)$$

and, for the sake of convenience, we have defined the following functions for the derivatives with respect to the trace T and the Ricci curvature scalar R

$$\mathcal{F}(R, T) \equiv \frac{\partial f(R, T)}{\partial T} \quad \text{and} \quad F(R, T) \equiv \frac{\partial f(R, T)}{\partial R}. \quad (6)$$

Assuming a perfect fluid and a spatially flat Friedmann–Lemaître–Robertson–Walker (FLRW) metric

$$ds^2 = -dt^2 + a^2(t)(dx^2 + dy^2 + dz^2), \quad (7)$$

together with using equation (4), the generalized Friedmann equation for a perfect fluid with non-zero pressure is achieved as

$$3H^2 F(R, T) + \frac{1}{2}\left(f(R, T) - F(R, T)R\right) + 3\dot{F}(R, T)H = \left(8\pi G + \mathcal{F}(R, T)\right)\rho + \mathcal{F}(R, T)p. \quad (8)$$

Applying the Bianchi identity to the field equation (4) leads to the following constraint for multi perfect fluids

$$\sum_{i=1}^{\mathcal{N}} \dot{\mathcal{F}}_i(R, T)(\rho_i + p_i) - \frac{1}{2}\mathcal{F}_i(R, T)(\dot{p}_i - \dot{\rho}_i) = 0, \quad (9)$$

where \mathcal{N} is the number of included perfect fluids. Constraint (9) for a pressure-less matter reduces to²

$$\dot{\mathcal{F}}(R, T) = \frac{3}{2}H(t)\mathcal{F}(R, T). \quad (10)$$

Equations (9) and (10) are two constraints that restrict the form of the Lagrangian density $f(R, T^{(\text{b}, \text{G})})$ in our case. These constraints guarantee the conservation of EMT which is imposed by the Bianchi identity³. Therefore, to obtain the Hubble parameter from equation (8), we need to find the function $f(R, T^{(\text{b}, \text{G})})$ that satisfy these constraints.

Generally, function $f(R, T^{(\text{b}, \text{G})})$ can take an arbitrary form in equations (8) and (9). As a matter of fact, viable models of $f(R, T)$ gravity can be classified in the following manner [77]

²For more details see Refs. [83, 84].

³Briefly, one can recast the field equations in a canonical form similar to GR. In this case, all the other terms can be realized as the matter terms, e.g. see Refs. [83, 84].

- The $f(R, T) = R + h(T)$ models which have been mostly considered in the literature. We can enumerate some motivations to propose these type of models; (i) equations of motion and the related calculations are more tractable in the framework of these models as compared to the other ones, such that one can always simply obtain the GR results by switching off the function $h(T)$. From mathematical point of view, in each theory modest field equations can result in exact solutions without resorting to numerical methods. (ii) these models can be seen as a trivial modification to GR which depends on the matter content (regardless of the simplest possibility, i.e., adding a cosmological constant). In this regard, a simple correction may lead to some plausible results comparing with the other type of corrections. These models may also connect to other theories, for example, those in which the cosmological constant clearly depends on the trace of EMT which is called “ $\Lambda(T)$ gravity” in the literature [120, 121, 122]. (iii) since any theory of modified gravity must be reduced to the Einstein-Hilbert action at low curvature regimes, for more complicated $f(R, T)$ functions, GR may not be recovered. (iv) these models are well-defined for cosmological fluids with $T = 0$, like radiation (as we will see the third type of models may show some inconsistencies). (v) the EMT conservation tells us that for a linear combination of curvature and matter sectors we can determine the form of $h(T)$ function up to some integration constants. However, for complicated forms, this option may not be accessible. Particularly, in our work the EMT conservation leads to an intricate function for the standard Chaplygin gas, see expression (29). Therefore a reasonable choice is to consider the contribution due to the trace of EMT into Lagrangian density, linearly. Such a setting makes calculations rough enough to take the Ricci scalar instead of an arbitrary function of it, as the geometrical part of the action.
- Models with arbitrary forms for the Ricci scalar but minimal coupling to the EMT trace: $f(R, T) = g(R) + h(T)$. These cases can be accounted for corrections on $f(R)$ gravity which may cure possible deficiencies of these theories. As some of the above motivations are still mentionable for these class of models, the complexities involved in the $g(R)$ function may lead to some problems such as finding exact solutions. In the present work, the benefit of choosing the simple form $g(R) = R$ is to obtain the Hubble parameter in terms of the matter terms, in a straightforward way. We note that the exact form of the Hubble parameter is needed in order to calculate the statefinder parameters, see e.g., equation (13). It is obvious that from equation (8), for cases in which $F(R, T) \neq \text{constant}$ the Hubble parameter may not be obtained exactly.
- The models with $f(R, T) = g_1(R) + h(T)g_2(R)$. The field equations for these type of models can be so complicated due to non-minimal coupling term. These categories suffer from an important problem. Since for an ultra relativistic fluid the trace of EMT is vanished, the models with non-minimal coupling between the geometrical and matter sectors in the La-

grangian can become singular. Optimistically, these cases reduce to $f(R)$ gravity similar to the cases discussed in the above items. For instance, the actions with a pure non-minimal term (i.e., $g_1(R) = 0$) can become either singular (eg., $h(T) \propto \text{Log}(T)$) or null, since the trace of ultra relativistic matter is vanished. Another issue is that, the excellent information about the function $h(T)$ which can be extracted from the models with linear combinations may be lost even for simple forms of $h(T)g_2(R)$. As a result, equation (10) turns into a completely complicated expression in terms of second time derivative of the Hubble parameter once non-minimal couplings are allowed. This in turn leaves us without any reasonable outcome for $h(T)$ function. The major concern of theories including non-minimal couplings in the Lagrangian is that they could lead to the violation of the equivalence principle [123].

Motivated by the above discussion, we consider a function of the following form

$$f(R, T^{(b, G)}) = R + h_1(T^{(b)}) + h_2(T^{(G)}). \quad (11)$$

Using definitions (6) and the ansatz (11) we get

$$\begin{aligned} \mathcal{F}_1(R, T^{(b, G)}) &= \frac{\partial f(R, T^{(b, G)})}{\partial T^{(b)}} = h_1'(T^{(b)}), \\ \mathcal{F}_2(R, T^{(b, G)}) &= \frac{\partial f(R, T^{(b, G)})}{\partial T^{(G)}} = h_2'(T^{(G)}), \\ F(R, T^{(b, G)}) &= \frac{\partial f(R, T^{(b, G)})}{\partial R} = 1, \end{aligned} \quad (12)$$

where the prime denotes a derivative with respect to the argument. Applying the derivatives (12) to equation (8) leaves us with the following relation

$$3H^2 = \sum_{i=1}^2 \left(8\pi G \rho_i + \mathcal{F}_i(\rho_i + p_i) - \frac{1}{2} h_i \right), \quad (13)$$

where the summation should be done over all terms corresponding to the two forms of matter. Notice that, hereafter the arguments in $\mathcal{F}_i(R, T^{(b, G)})$, $h_1(T^{(G)})$ and $h_2(T^{(b)})$ will be dropped for simplicity until we may restore them for some purposes.

For a perfect fluid with $p = p(\rho)$, the constraint (9) using the trace $T = -\rho + 3p(\rho)$ and the conservation equation $\dot{\rho} + 3H(\rho + p) = 0$, could in principle leads to a differential equation for the function $f(R, T)$. For the expression (11) it reads

$$\left(\dot{h}_1' \rho^{(b)} + \frac{1}{2} h_1' \dot{\rho}^{(b)} \right) + \left[\dot{h}_2' (\rho^{(G)} + p^{(G)}) - \frac{1}{2} h_2' (\dot{p}^{(G)} - \dot{\rho}^{(G)}) \right] = 0. \quad (14)$$

Therefore, assuming that the two matters do not interact with each other, we can obtain

$$\dot{h}'_1 \rho^{(b)} + \frac{1}{2} h'_1 \dot{\rho}^{(b)} = 0, \quad (15)$$

$$\dot{h}'_2 (\rho^{(G)} + p^{(G)}) - \frac{1}{2} h'_2 (\dot{p}^{(G)} - \dot{\rho}^{(G)}) = 0. \quad (16)$$

Since the signature of metric (7) implies $\rho^{(b)} = -T^{(b)}$ for the pressureless matter, equation (15) gives

$$h_1(T^{(b)}) = C_1^{(b)} \sqrt{-T^{(b)}} + C_2^{(b)}. \quad (17)$$

where $C_1^{(b)}$ and $C_2^{(b)}$ are constants of integration. Now we try to solve equation (16) for GCG. The EoS for GCG is written as

$$P^{(G)} = -\frac{A}{\rho^{(G)\alpha}}. \quad (18)$$

Equation (18) together with the equation of the EMT conservation $\dot{\rho}^{(G)} + 3H(\rho^{(G)} + p^{(G)}) = 0$ lead to the following solution for the matter density of GCG

$$\rho^{(G)} = (A + Ba^{-3(1+\alpha)})^{\frac{1}{1+\alpha}}, \quad (19)$$

where A , α and B are some constant which have to satisfy the conditions $A > 0$ and $\alpha \geq 0$ ⁴. Setting $\rho_0^{(G)} \equiv \rho^{(G)}(a = 1)$, we can rewrite (19) in a suitable form as

$$\rho^{(G)} = \rho_0^{(G)} \left(K + (1 - K)a^{-3(1+\alpha)} \right)^{\frac{1}{1+\alpha}}, \quad (20)$$

where a is the scale factor and $K \equiv A/\rho_0^{(G)(1+\alpha)}$. For later applications we rewrite (20) as

$$\rho^{(G)} = \rho_0^{(G)} u(a; \alpha, K), \quad (21)$$

where

$$u(a; \alpha, K) \equiv \left(K + (1 - K)a^{-3(1+\alpha)} \right)^{\frac{1}{1+\alpha}}, \quad (22)$$

where $u(1; \alpha, K) = 1$. Note that, the argument $(a; \alpha, K)$ denotes the variation with respect to the scale factor for constant values of α and K . Substituting equation (18) in (16) together with using $\dot{\rho}^{(G)} + 3H(\rho^{(G)} + p^{(G)}) = 0$ and $T^{(G)} = -\rho^{(G)} + 3p^{(G)}$, we get

$$2 \frac{h''_2}{h'_2} = \frac{\rho^{(G)} + \alpha p^{(G)}}{(\rho^{(G)} + 3\alpha p^{(G)})(\rho^{(G)} + p^{(G)})}. \quad (23)$$

⁴These restrictions come from the GCG sound speed considerations. See, e.g., Ref. [52].

The left hand side of equation (23) is in terms of $T^{(G)}$ while the right hand side is a function of $\rho^{(G)}$ and $p^{(G)}$, which shows that it is not a closed differential equation. To complete it, the trace of EMT of GCG can be rewritten as the following form

$$-\rho^{(G)} - 3\frac{A}{\rho^{(G)}\alpha} = T^{(G)}. \quad (24)$$

By solving equation (24), in principle, we can obtain the matter density $\rho^{(G)}$ in terms of the GCG trace, and then, substitute it into equations (18) and (23) to get a closed differential equation in terms of the pure trace $T^{(G)}$. Unfortunately, this is not a straightforward calculation, since equation (24) admits a lot of roots that depend on the value α (equation (24) can be problematic when non-integer values of α are included as well). Furthermore, the solutions can get complicated forms such that the differential equation (23) may not be solved. However, for the case of the standard Chaplygin gas (SCG), namely, $\alpha = 1$ the solutions are tractable and for the other values we use the approximation methods. Equation (24) for $\alpha = 1$ has the following solutions

$$\rho_{\pm}^{(S)} = \frac{1}{2} \left(-T^{(S)} \pm \sqrt{-12A + T^{(S)2}} \right), \quad (25)$$

where superscript "S" stands for SCG. Since, $\rho_{-}^{(S)}$ can get negative values and thus violates the weak energy condition (WEC), we discard it as a non-physical solution. We then consider the solution $\rho_{+}^{(S)}$. By setting $\alpha = 1$ in equation (23), and using (25) we have

$$2\frac{h''_{2,+}}{h'_{2,+}} = \frac{1}{(2\rho_{+}^{(S)} + T^{(S)})} = \frac{1}{\sqrt{-12A + T^{(S)2}}}, \quad (26)$$

and, we finally obtain the following differential equation

$$2\sqrt{-12A + T^{(S)2}}h''_{2,+} - h'_{2,+} = 0, \quad (27)$$

where the solution $h_{2,+}$ corresponds to $\rho_{+}^{(S)}$. The solutions of the above differential equation are obtained as

$$h_{2,+}(T^{(S)}) = -\frac{2}{3}C_{1+}^{(S)} \left(-2T^{(S)} + \sqrt{-12A + T^{(S)2}} \right) \sqrt{T^{(S)} + \sqrt{-12A + T^{(S)2}}} + C_{2+}^{(S)}, \quad (28)$$

where $C_{1+}^{(S)}$ and $C_{2+}^{(S)}$ are constants of integration. As a result, in $f(R, T)$ theory of gravity, for the non-interacting baryonic matter and SCG, the conservation of EMT enforces us to use the following function

$$\begin{aligned} f^{(I)}(R, T^{(b, S)}) &= R + C_1^{(b)} \sqrt{-T^{(b)}} \\ &- \frac{2}{3}C_1^{(S)} \left(-2T^{(S)} + \sqrt{-12A + T^{(S)2}} \right) \sqrt{T^{(S)} + \sqrt{-12A + T^{(S)2}}} + \Lambda^{(b, S)}, \end{aligned} \quad (29)$$

where we have restored the argument of function f for clarification and dropped the sign "+". Also, we have added the superscript I for later applications and $\Lambda^{(b,S)} \equiv C_2^{(b)} + C_2^{(S)}$. Nevertheless, we consider two another model; the models which use GCG in two extreme situations, i.e., when $p^{(G)} \gg \rho^{(G)}$ and $\rho^{(G)} \gg p^{(G)}$. These cases will be considered for arbitrary values of α . In either cases we approximate $T_p^{(G)} \simeq 3p^{(G)} = -3|p^{(G)}|$ and $T_\rho^{(G)} \simeq -\rho^{(G)}$. In these cases, using equation (16), the related differential equations are given as

$$2T_p^{(G)}h_{2,p}''(T_p^{(G)}) - h_{2,p}'(T_p^{(G)}) \simeq 0, \quad (30)$$

$$2T_\rho^{(G)}h_{2,\rho}''(T_\rho^{(G)}) + h_{2,\rho}'(T_\rho^{(G)}) \simeq 0, \quad (31)$$

for which the solutions are found as

$$h_{2,p}(T_p^{(G)}) = \frac{2}{3}C_{1p}^{(G)}(-T_p^{(G)})^{3/2} + C_{2p}^{(G)}, \quad (32)$$

and

$$h_{2,\rho}(T_\rho^{(G)}) = 2C_{1\rho}^{(G)}\sqrt{-T_\rho^{(G)}} + C_{2\rho}^{(G)}, \quad (33)$$

where we have restored again the arguments and labeled the equations and solutions by p and ρ that denote the either extreme cases and $C_{ip}^{(G)}$ and $C_{i\rho}^{(G)}$ with $i = 1, 2$ are integral constants. Thus, we have two another forms for $f(R, T)$ function, i.e.,

$$f^{(II)}(R, T^{(b, G)}) = R + C_1^{(b)}\sqrt{-T^{(b)}} + \frac{2}{3}C_{1p}^{(G)}(-T^{(G)})^{3/2} + \Lambda_p^{(b, G)}, \quad (34)$$

for $|p^{(G)}| \gg \rho^{(G)}$, where $\Lambda_p^{(b, G)} \equiv C_2^{(b)} + C_{2p}^{(G)}$ and

$$f^{(III)}(R, T^{(b, G)}) = R + C_1^{(b)}\sqrt{-T^{(b)}} + 2C_{1\rho}^{(G)}\sqrt{-T^{(G)}} + \Lambda_\rho^{(b, G)}, \quad (35)$$

for $\rho^{(G)} \gg |p^{(G)}|$, where $\Lambda_\rho^{(b, G)} \equiv C_2^{(b)} + C_{2\rho}^{(G)}$. Note that, there are two sets of constants labeled by the numbers 1 and 2 which determine the degree of involved differential equations.

Therefore, we have three classes of non-interacting models including pressureless baryonic and three forms of CG; in the first one we have SCG represented by the function (29), the second one uses GCG when the matter density is negligible in comparison with the pressure as shown by the function (34), and in the last case, the GCG matter density is dominant which is determined by function (35).

Note that, from equations (18) and (20), the EoS parameter $w^{(GCG)}$ for GCG can be obtained. At the early time ($a \rightarrow 0$), we have $w^{(GCG)} \rightarrow 0$, and at the late time ($a \rightarrow \infty$), $w^{(GCG)} \rightarrow -1$. This means that the GCG in the early time behaves like CDM and in the late time like DE. Therefore, we assume that DE and CDM are unified by GCG model. Besides, we have the baryonic matter indicated by superscript "b" which does not interact with GCG component.

In the next section, we present the statefinder parameters and obtain them for these three models, and also get the deceleration parameter and define the effective EoS, as well. Henceforth, we will call these as, models I, II and III.

3 Statefinder parameters and the related definitions

In this section, we present the definitions of the statefinder parameters and calculate them for models I, II and III. These parameters are important to discuss the cosmological aspects of models which are introduced in Refs. [105, 106], originally. The statefinder parameters are defined via the following pairs of parameters [105, 106]

$$r \equiv \frac{\ddot{a}}{a} H^{-3}, \quad (36)$$

$$s \equiv \frac{r - 1}{3(q - 1/2)}. \quad (37)$$

Models that have the same present values of the Hubble parameter H_0 and the deceleration parameter q_0 , can be discriminated from each other by these parameters. These parameters include the third time derivative of the scale factor (in spite of the Hubble parameter which includes the first time derivative and the deceleration parameter which includes the second time derivative of the scale factor) and can be used to distinguish the different DE models. The deceleration parameter is defined as the first time derivative of the Hubble parameter, i.e.,

$$q \equiv -\frac{\dot{H}}{H^2} - 1, \quad (38)$$

which in terms of the normalized Hubble parameter $E(a) = H/H_0$, it can be rewritten as

$$q = -\frac{1}{E} \frac{dE}{dN} - 1, \quad (39)$$

where $N \equiv \ln a$. Using the definition (38), the statefinder parameter r can be simply calculated as

$$r = q(1 + 2q) - \frac{dq}{dN}, \quad (40)$$

whereby substituting (39) in (40) gives

$$r = \frac{1}{E} \frac{d^2 E}{dN^2} + \frac{1}{E^2} \left(\frac{dE}{dN} \right)^2 + \frac{3}{E} \frac{dE}{dN} + 1. \quad (41)$$

One can use equations (39) and (41) to obtain the statefinder parameter s from definition (37). According to the definition of the normalized Hubble parameter, and also using (13) for models (29), (34) and (35) we obtain

$$E^{(I)}(a; 1, K) = \left[\Omega_0^{(b)} (1 - \mathbf{m}a^{3/2}) a^{-3} + \Omega_0^{(S)} u(a; 1, K) \left(1 - \sqrt{24\mathbf{n}^{(I)}} \left(\frac{u(a; 1, K)}{K} \right)^{-3/2} \right) \right]^{\frac{1}{2}}, \quad (42)$$

$$E^{(II)}(a; \alpha, K) = \left[\Omega_0^{(b)} (1 - \mathbf{m}a^{3/2}) a^{-3} + \Omega_0^{(G)} u(a; \alpha, K) \left(1 - \sqrt{12\mathbf{n}^{(II)}} K^{\frac{3}{2}} u(a; \alpha, K)^{-\frac{3\alpha+2}{2}} \right) \right]^{\frac{1}{2}}, \quad (43)$$

and

$$E^{(III)}(a; \alpha, K) = \left[\Omega_0^{(b)} (1 - \mathbf{m}a^{3/2}) a^{-3} + \Omega_0^{(G)} u(a; \alpha, K) \left(1 - 2\mathbf{n}^{(III)} u(a; \alpha, K)^{-\frac{1}{2}} \right) \right]^{\frac{1}{2}}, \quad (44)$$

where we have defined the density parameters for the two type of fluids and some dimensionless parameters, as

$$\begin{aligned} \Omega_0^{(b)} &= \frac{8\pi G \rho_0^{(b)}}{3H_0^2}, & \Omega_0^{(S/G)} &= \frac{8\pi G \rho_0^{(S/G)}}{3H_0^2}, & \mathbf{m} &= \frac{\rho_0^{(b) -1/2} C_1^{(b)}}{8\pi G}, \\ \mathbf{n}^{(I)} &= \frac{\rho_0^{(S) 1/2} C_1^{(S)}}{8\pi G}, & \mathbf{n}^{(II)} &= \frac{\rho_0^{(G) 1/2} C_{1\rho}^{(G)}}{8\pi G}, & \mathbf{n}^{(III)} &= \frac{\rho_0^{(G) -1/2} C_{1\rho}^{(G)}}{8\pi G}. \end{aligned} \quad (45)$$

Hence, each model includes some parameters; the space parameters of model I are $(\mathbf{m}, \mathbf{n}^{(I)}, K)$, those of model II are $(\mathbf{m}, \mathbf{n}^{(II)}, K, \alpha)$ and for model III we have $(\mathbf{m}, \mathbf{n}^{(III)}, K, \alpha)$. These parameters play the role of some tuners for these models which can be set for a physically interesting situation. Substituting equations (42), (43) and (44) in equation (39) gives the related deceleration parameters as

$$q^{(I)} = \frac{3}{4E^{(I),2}} \left[\Omega_0^{(b)} (2 - \mathbf{m}a^{3/2}) a^{-3} + 2\Omega_0^{(S)} (1 - K) uv \left(1 + \sqrt{6\mathbf{n}^{(I)}} (u/K)^{-3/2} \right) \right] - 1, \quad (46)$$

$$q^{(II)} = \frac{3}{4E^{(II),2}} \left[\Omega_0^{(b)} (2 - \mathbf{m}a^{3/2}) a^{-3} + 2\Omega_0^{(G)} (1 - K) v \left(u + \sqrt{27\alpha\mathbf{n}^{(II)}} \left(\frac{u^\alpha}{K} \right)^{-3/2} \right) \right] - 1, \quad (47)$$

and

$$q^{(III)} = \frac{3}{4E^{(III),2}} \left[\Omega_0^{(b)} (2 - \mathbf{m}a^{3/2}) a^{-3} + 2\Omega_0^{(G)} (1 - K) uv \left(1 - \mathbf{n}^{(III)} u^{-\frac{1}{2}} \right) \right] - 1, \quad (48)$$

for models I, II and III, respectively. It is convenient to define an effective EoS in the higher order gravity (specially in $f(R)$ gravity) to explain the present accelerated expansion of the Universe through the effects of the geometrically modified gravity terms in the Friedmann equations⁵. Here, we have not taken into account such modifications in the geometrical sector of the action. However, there is a non-standard interaction between cosmological fluids and normal geometrical sector, which is the general behavior of $f(R, T)$ gravity. The effective EoS parameter $w^{(\text{eff})}$ is defined as $w^{(\text{eff})} = -1 - 2\dot{H}/3H^2$ ⁶, whereby using the definition (38) we get,

$$w^{(\text{eff})} = \frac{1}{3}(2q - 1). \quad (49)$$

The effective EoS can be obtained from equations (46), (47), (48) and (49) for the three models. Using equations (41), (42), (43) and (44) the statefinder parameters r can be calculated as

$$r^{(\text{I})} = \frac{9}{8E^{(\text{I}),2}} \left\{ \Omega_0^{(\text{b})} \mathbf{m} a^{-3/2} + \Omega_0^{(\text{S})} (1 - K) u^{-1} v \left[4K + \sqrt{24} \mathbf{n}^{(\text{I})} \left(2 - 5(1 - K)v \right) (u/K)^{-3/2} u^2 \right] \right\} + 1, \quad (50)$$

$$r^{(\text{II})} = \frac{9}{8E^{(\text{II}),2}} \left\{ \Omega_0^{(\text{b})} \mathbf{m} a^{-3/2} + 2\alpha \Omega_0^{(\text{G})} (1 - K) v \left[2 \left(1 - (1 - K)v \right) u + \sqrt{27} \mathbf{n}^{(\text{II})} \left(2\alpha - (1 - K)(2 + 5\alpha)v \right) \left(\frac{u^\alpha}{K} \right)^{-3/2} \right] \right\} + 1, \quad (51)$$

$$r^{(\text{III})} = \frac{9}{8E^{(\text{III}),2}} \left\{ \Omega_0^{(\text{b})} \mathbf{m} a^{-3/2} + 2\Omega_0^{(\text{G})} (1 - K) v u \left[2\alpha \left(1 - (1 - K)v \right) - \mathbf{n}^{(\text{III})} \left(2\alpha - (1 - K)(1 + 2\alpha)v \right) u^{-\frac{1}{2}} \right] \right\} + 1, \quad (52)$$

and the statefinder s for three models can be computed from definition (37), using the above equations for the deceleration parameters $q^{(\text{I})}, q^{(\text{II})}, q^{(\text{III})}$ and the statefinder parameters $r^{(\text{I})}, r^{(\text{II})}, r^{(\text{III})}$, as

$$s^{(\text{I})} = \frac{1}{2} \frac{\Omega_0^{(\text{b})} \mathbf{m} a^{-3/2} + \Omega_0^{(\text{S})} (1 - K) u^{-1} v \left[4K + \sqrt{24} \mathbf{n}^{(\text{I})} \left(2 - 5(1 - K)v \right) (u/K)^{-3/2} u^2 \right]}{\Omega_0^{(\text{b})} \mathbf{m} a^{-3/2} - \Omega_0^{(\text{S})} u^{-1} \left[2K - \sqrt{24} \mathbf{n}^{(\text{I})} \left(2 + (1 - K)v \right) (u/K)^{-3/2} u^2 \right]}, \quad (53)$$

⁵For example, see Ref. [119] and references therein.

⁶See Refs. [83, 84]

$$s^{(\text{II})} = \frac{1}{2} \frac{\Omega_0^{(\text{b})} \mathbf{m} a^{-3/2} + 2\alpha \Omega_0^{(\text{G})} (1-K)v \left[2(1-(1-K)v)u + \sqrt{27}\mathbf{n}^{(\text{II})} (2\alpha - (1-K)(2+5\alpha)v) \left(\frac{u^\alpha}{K}\right)^{-\frac{3}{2}} \right]}{\Omega_0^{(\text{b})} \mathbf{m} a^{-3/2} - \Omega_0^{(\text{G})} \left[2(1-(1-K)v)u - \sqrt{12}\mathbf{n}^{(\text{II})} (2+3\alpha(1-K)v) \left(\frac{u^\alpha}{K}\right)^{-\frac{3}{2}} \right]}, \quad (54)$$

$$s^{(\text{III})} = \frac{1}{2} \frac{\Omega_0^{(\text{b})} \mathbf{m} a^{-3/2} + 2\Omega_0^{(\text{G})} (1-K)vu \left[2\alpha(1-(1-K)v) - \mathbf{n}^{(\text{III})} (2\alpha - (1-K)(1+2\alpha)v) u^{-\frac{1}{2}} \right]}{\Omega_0^{(\text{b})} \mathbf{m} a^{-3/2} - 2u\Omega_0^{(\text{G})} \left[1 - (1-K)v - \mathbf{n}^{(\text{III})} (2 - (1-K)v) u^{-\frac{1}{2}} \right]}, \quad (55)$$

where we have defined $v(a; \alpha, K) = [a^3 u(a; \alpha, K)]^{-(1+\alpha)}$, and also dropped the arguments $(a; 1, K)$ and $(a; \alpha, K)$ from the quantities of model I and the two other ones, respectively. Note that, the dimensionless parameters introduced in (45) are not independent. Applying the present value $E_0^{(\text{I})}(1; \alpha, K) = 1$, and also the same for the other models, we get

$$\Omega_0^{(\text{S})} = \frac{1 - (1 - \mathbf{m})\Omega_0^{(\text{b})}}{1 - \sqrt{12}\mathbf{n}^{(\text{I})} K^{\frac{3}{2}}} \quad \text{for model I,} \quad (56)$$

$$\Omega_0^{(\text{G})} = \frac{1 - (1 - \mathbf{m})\Omega_0^{(\text{b})}}{1 - \sqrt{24}\mathbf{n}^{(\text{II})} K^{\frac{3}{2}}} \quad \text{for model II,} \quad (57)$$

$$\Omega_0^{(\text{G})} = \frac{1 - (1 - \mathbf{m})\Omega_0^{(\text{b})}}{1 - 2\mathbf{n}^{(\text{III})}} \quad \text{for model III.} \quad (58)$$

Setting $\mathbf{m} = 0$ and \mathbf{n} 's = 0, in equations (46)-(55) and also relations (56)-(58) gives the corresponding equations for model $f(R, T) = R$, i.e. the GR case. These coupling constants are responsible for all deviations of the above equations from the equivalent forms in GR. In the next section we study these deviations for three models I, II and III, numerically. That is, we investigate the cosmological consequences of equations (46)-(55) through the statefinder diagnosis.

4 Statefinder diagnosis and numerical considerations

In this section we consider equations (46)-(55) and extract their cosmological consequences via the statefinder diagnosis. These three models depend on the coupling constants \mathbf{m} and \mathbf{n} 's, and also parameter K for model I, and K, α for the two other ones. Generally, these constants can lead to different models for different values, and therefore, different cosmological history for the universe. In the following subsections we consider each model, in turn.

Note that, in each forthcoming diagram, the trajectories of cosmological parameters for $\mathbf{m}, \mathbf{n}'=0$ correspond to the GR background. Namely, one can compare the $f(R, T)$ gravity results with the corresponding GR ones in each model I, II and III, using these plots.

Later, in Sec. 5, we compare the predicted present values s_0 and j_0 by our models (which have been obtained for the best fit values of models parameters), to some observational measurements. The gold sample supernova type Ia which gives $1.65 < r_0 < 3.97$ [92], the SNLS supernova type Ia data set which results in $0.11 < r_0 < 2.69$ [93] and X-ray galaxy clusters analysis which gives $-1.49 < r_0 < 3.06$ [94] have been used. Future measurements like SNIa data from the Large Synoptic Survey Telescope (LSST), the Supernovae Acceleration Probe (SNAP) and X-ray cluster data from Constellation-X may provide better constraints on the statefinder parameters. The baryon oscillation experiment which is applied in galaxy redshift surveys for high-redshift ranges can also make tighter constraint on these parameters.

4.1 model $f^{(I)}(R, T^{(\mathbf{b}, \mathbf{S})})$

Using equations (46) and (49), the cosmological evolution of the EoS parameter for this model is illustrated in Fig. 1, for specific values $K = 0, 0.33, 0.77$ and 0.99 with $\mathbf{m}, \mathbf{n}^{(I)} = -1$. Moreover, we have plotted the corresponding diagrams for the standard case $\mathbf{m} = 0, \mathbf{n}^{(I)} = 0$ (i.e., for GR, as we have before mentioned) in order to indicate possible deviations. The zero value for K , corresponds to the model with a pressureless matter (see equation (20)), and the other values determine different cosmological scenarios. The predicted present value $w_0^{(\text{eff})}$, is indicated by a solid circle on each curve. Also, we have illustrated observational range for the values of EoS parameter of DE which has been reported by Planck 2015 measurements [33], ($-1.051 \leq w_{0, \text{Planck}}^{(\text{eff})} \leq -0.961$), in Fig. 1 by a gray region. Brown dashed line has been used for case $K = 0$, blue dotted one for $K = 0.33$, red dot-dashed curve shows the case $K = 0.77$, a black line presents the models with $K = 0.99$ and an orange one for $K = 1$ ⁷. Since, there are generally some divergences in the cases with positive values of $\mathbf{n}^{(I)}$ and \mathbf{m} (which occur in a certain value of N , for some values of K), the evolution of the related EoS parameter is not depicted in Fig. 1. Physically, this divergence causes a total increase in the value of the deceleration parameter after the matter dominated era⁸. Hence, positive values for the coupling constants $\mathbf{m}, \mathbf{n}^{(I)}$, can lead to non-physical behaviors and we discard such cases as the less physically interesting models. However, one may find some curves without divergence for positive values. For example, for $\mathbf{m} = 2, \mathbf{n}^{(I)} = -2.3$ and $K = 0.32$ we can obtain the acceptable value $w^{(\text{eff})} \simeq -1.005$ consistent with the recent results [11, 33]. Plots in Fig. 1 show that the value of the effective EoS is much more near to its observationally obtained values, $w^{(\text{obs})} \simeq -1$, for $\mathbf{n}^{(I)} \neq 0$. Decreasing the

⁷In the subsequent discussions and subsections we always use these options to show the related plots for $K = 0, 0.33, 0.77, 0.99$.

⁸Note that, for this reason, we do not consider the other cosmological parameters for this model and also for two other ones for positive valued parameters \mathbf{m}, \mathbf{n}' s.

parameter $\mathbf{n}^{(1)}$ for $\mathbf{m} = 0$, leads to smaller values of $w^{(\text{eff})}$ for all values of K . By contrast, decreasing in the parameter \mathbf{m} for $\mathbf{n}^{(1)} = 0$, gives smaller values for $K < 1/2$ and larger values for $K > 1/2$. To understand the reason of this dual behavior, we calculate the present value of $w^{(\text{eff})}$ for $\mathbf{n}^{(1)} = 0$, as

$$w_0^{(\text{eff})} = K(\Omega_0^{(b)} - 1) - \frac{1}{2}(2K - 1)\mathbf{m}\Omega_0^{(b)}, \quad \mathbf{n}^{(1)} = 0, \quad N = 0. \quad (59)$$

As we see, for special case $K = 1/2$, the effective EoS is independent of the parameter \mathbf{m} and for a given \mathbf{m} , the value of $w_0^{(\text{eff})}$ increases for $K > 1/2$ and decreases for $K < 1/2$. Calculations show that when $\mathbf{n}^{(1)} \neq 0$, the mutual behavior is absent and in these situations a decrease in \mathbf{m} leads to an increase in $w_0^{(\text{eff})}$ for all values of K (compare lower diagrams in Fig. 1). Therefore, in lower right diagram we see a total decrease in the value of $w_0^{(\text{eff})}$ (a decrease due to the effect of $\mathbf{n}^{(1)} \neq 0$ and an increase due to the effect of \mathbf{m}). The value of $w_0^{(\text{eff})}$ vanishes in the early times ($N < 0$ which corresponds to $a < 1$), and goes to -1 in the late times except for the case $K = 0$.

The evolution of the deceleration parameter (46) is presented in Fig. 2. An interesting result is that, the value of the deceleration parameter for the models with $K = 0$ is running when $\mathbf{m} < 0$. The curve corresponding to $K = 0$, is sensitive to negative values of \mathbf{m} . Plots show that there is a transition between the value $1/2$ and negative values of q . This transition for $K = 0$ is relatively slower than for the other value of K ; the larger values the parameter \mathbf{m} gets, the later the transition occurs. In addition to the mentioned effect of negative values of \mathbf{m} for curves with $K = 0$, the overall effects of the parameters \mathbf{m} and $\mathbf{n}^{(1)}$ can be distinguished. To this end, the present values of the deceleration function q_0 in Fig. 2 (and the statefinder parameters r_0 and s_0 in Fig. 3), are specified for some curves. Comparing upper left corner diagram with lower left one in Fig. 2, shows that the net effect of $\mathbf{n}^{(1)} (< 0)$ is to decrease the values of q_0 . Since there is a linear relation between the deceleration and EoS parameters, there exists a similar mutual behavior for the effect of \mathbf{m} when $\mathbf{n}^{(1)} = 0$.

In Fig. 3, we present the evolution of the statefinder parameters in the (s, r) plane for $K = 0.33, 0.77, 0.99$. In this plane, the values of s are mapped on a horizontal axis and a vertical axis determines the values of r . In the upper left panel, we plot the diagrams that hold for GR, in order to see possible deviations. In each panel besides the present values (which are indicated by small solid circle), we represent starting point with a star symbol (corresponding to a point in the early times), the position of the Λ CDM model (corresponding to future) with a solid small box and the direction of the evolution of the trajectories with colored arrows. The starting point corresponding to the early times is obtained by the condition $a \rightarrow 0$. In the limit $a \rightarrow 0$, the statefinder parameter r reads

$$r^{(1)}(a \rightarrow 0) = 1 + \frac{9\mathbf{m}\Omega_0^{(b)}a^{3/2}}{8\left(\Omega_0^{(b)} - \frac{\sqrt{1-K}(1+(\mathbf{m}-1)\Omega_0^{(m)})}{2\sqrt{6}K^{3/2}\mathbf{n}^{(1)}-1}\right)}, \quad (60)$$

whence, for the early times we get $r = 1$. However, the limit of s for $a \rightarrow 0$ depends on the value of the parameters \mathbf{m} and $\mathbf{n}^{(1)}$; for zero value for both

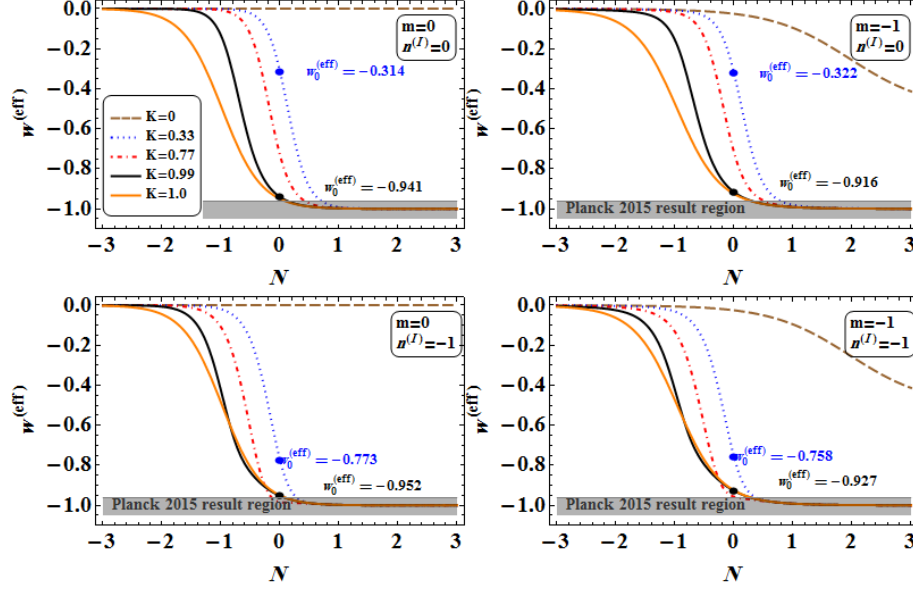


Figure 1: (color online). The cosmological evolution of the effective EoS parameter of model I versus $N \equiv \ln a$. The curves are plotted for $K = 0$ (which in this case we have CDM in addition to the baryonic one) in brown dashed line, blue dotted line for $K = 0.33$, red dot-dashed line for case $K = 0.77$, black solid line for $K = 0.99$ and orange solid line for $K = 1.00$. Small solid circles determine the present values. The valid range of values which has been reported by Planck 2015 measurements, $(-1.051 \leq w_{0, \text{Planck}}^{(\text{eff})} \leq -0.961)$ is also indicated by the gray region. All diagrams are drawn for the present baryonic matter density $\Omega_0^{(b)} = 0.05$. Since, positive values of parameters \mathbf{m} and $\mathbf{n}^{(I)}$ lead to some abnormality, only negative values are discussed. The curve of $K = 1.00$ is not flat because of the effect of the baryonic matter density. Zero value for the coupling constants \mathbf{m} and $\mathbf{n}^{(I)}$ reflects the GR background. Columnar view shows that decreasing the value of $\mathbf{n}^{(I)}$ leads to decreasing the present values. However, lateral view demonstrates that decreasing \mathbf{m} leads to an increase for $K > 0.5$ and a decrease for $K < 0.5$. An orthogonal look shows that the overall effect of switching on both parameter leads to more observationally accepted values for $K < 0.5$. For larger values of \mathbf{m} and $\mathbf{n}^{(I)}$ we get the better results.

parameters we have $s = -1$, if only the former is vanished $s = -1/2$, and otherwise we have $s = +1/2$. Therefore, for non-interacting SCG and baryonic matter, in the background of $f(R, T)$ theory of gravity, the trajectories of the statefinder plane belongs to three different subclasses; some trajectories have the initial value $(s = -1, r = 1)$, and the other two have $(s = \pm 1/2, r = 1)$, as the initial values. However, all trajectories terminate at the Λ CDM fixed point, since the statefinder parameters in the limit $a \rightarrow \infty$ take the following forms

$$r^{(I)}(a \rightarrow \infty) = 1 + \mathcal{C}_1(K, \mathbf{m}, \mathbf{n}^{(I)}, \Omega_0^{(b)})a^{-3/2}, \quad (61)$$

$$s^{(I)}(a \rightarrow \infty) = \mathcal{C}_2(K, \mathbf{m}, \mathbf{n}^{(I)}, \Omega_0^{(b)})a^{-3/2}, \quad (62)$$

where \mathcal{C}_1 and \mathcal{C}_2 are some functions of their arguments. Here, in model I, there

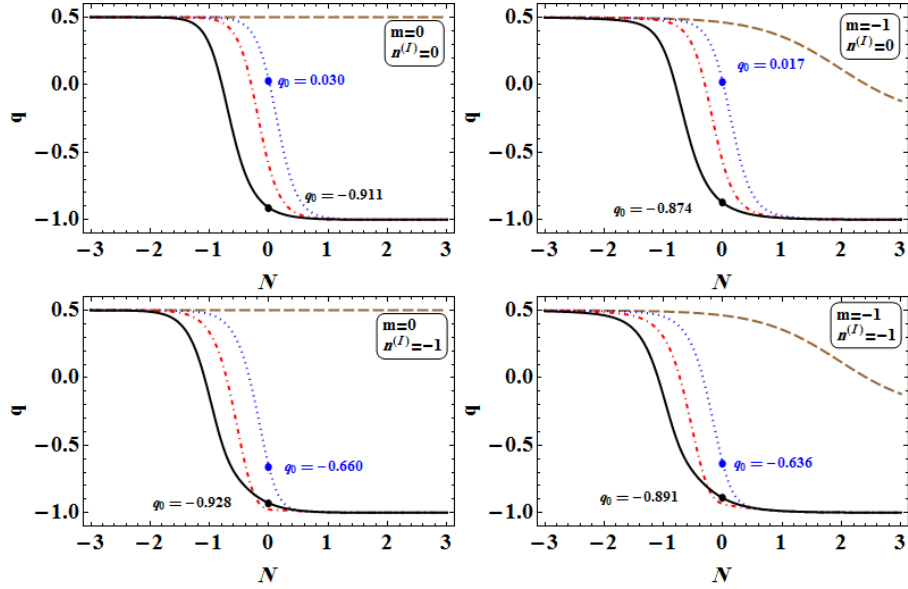


Figure 2: (color online). The evolution of the deceleration parameter of model I for different negative values of the parameters \mathbf{m} and $\mathbf{n}^{(1)}$. The curves are plotted for $K = 0$, $K = 0.33$, $K = 0.77$ and $K = 0.99$ corresponding to brown dashed line, blue dotted line for, red dot-dashed line and black solid line. Moreover, present values indicated by small solid circles. All diagrams are drawn for the present baryonic matter density $\Omega_0^{(b)} = 0.05$. The case $K = 0$ corresponds to the presence of only the baryonic and CDM. In this case, the deceleration parameter is constant 0.5 in GR (which corresponds to $\mathbf{m}, \mathbf{n}^{(1)} = 0$). On the contrary, decreasing the value of \mathbf{m} leads to a varying deceleration parameter in $f(R, T)$ gravity. By decreasing both parameters, we obtain better results for the only cases with $K < 0.5$, however, decreasing only in $\mathbf{n}^{(1)}$ improves the result for all values $0 < K < 1$.

are different scenarios for the evolution of the Universe, with more or less the same feature in their deceleration parameters, but completely different feature in the (r, s) plane; the Universe begins with different initial points, however, terminates in the same point in the late times, mimicking the cosmological constant mode. Lateral comparison of diagrams in Fig. 3, shows that for a specific value of K , the net effect of negative values of \mathbf{m} is an increase in the value of s_0 , and a decrease in the value of r_0 . A columnar view shows that negative values of $\mathbf{n}^{(1)}$ would increase the value of s_0 . Nevertheless, in these cases the value of r_0 grows for $0.17 < K < 0.33$ (the maximum value $r_{0,max} \simeq 1.76$ occurs in $K \simeq 0.24$), and decreases otherwise. Diagonal comparison demonstrates that the distance to the Λ CDM fixed point is shorter when both parameters \mathbf{m} and $\mathbf{n}^{(1)}$ are turned on. Such an effect is not seen for large K ; negative values of \mathbf{m} and $\mathbf{n}^{(1)}$ makes the distance of the model to the Λ CDM fixed point slightly larger comparing with GR. However, the models with $K \rightarrow 1$ have shorter distance.

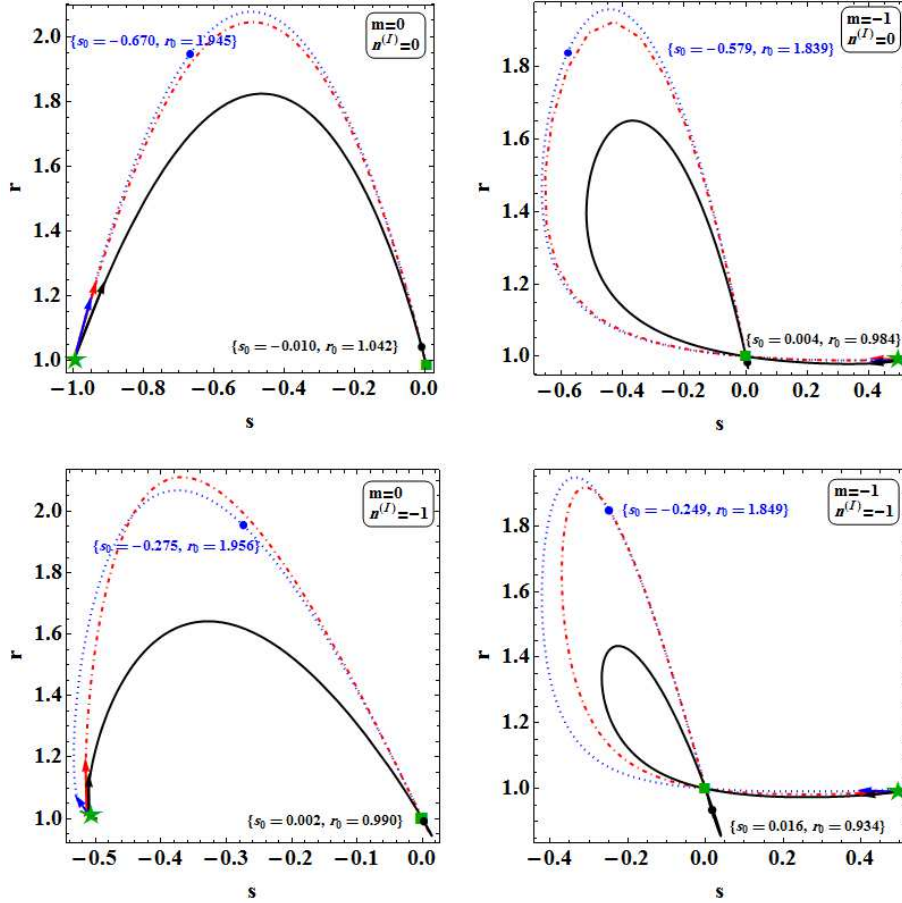


Figure 3: (color online). Statefinder diagnosis of model I in the (s, r) plane. In this plane the parameter r corresponds to the vertical axis and the values of parameter s form the horizontal axis. Each trajectory start from a star symbol and end up at a boxed symbol. The star symbol denotes the initial value for the trajectories. There is three different cases; some trajectories start from $(-1, 1)$ (upper left panel), some start from $(-0.5, 1)$ (lower left panel) and other trajectories begin from $(+0.5, 1)$ (right diagrams). However, all trajectories terminate at the boxed symbol place with coordinate $(0, 1)$ which belongs to the Λ CDM model. The diagram in lower right panel shows that decreasing the values of m and $n^{(I)}$ reduces the distance to the Λ CDM fixed point which for $K > 0.5$ is not very effective.

4.2 model $f^{(\text{II})}(R, T^{(\text{b}), \mathbf{G}})$

In this case besides the model coupling constants $\mathbf{m}, \mathbf{n}^{(\text{II})}$ and parameter K , there is another parameter, α , as the fourth constant. Therefore, the net effects of this parameter should be considered. The related figures of the effective EoS parameter $w^{(\text{eff})}$ for this model are illustrated in Fig. 4. Again, the curves for $K = 0, 0.33, K = 0.77$ and $K = 0.99$, corresponding to brown dashed, blue dotted, red dot-dashed and black solid lines are plotted, respectively. Here, the diagrams for $\alpha = 0.001, 0.99$ are drawn. It is clear from equations (46), (47) and (48), that the deceleration and accordingly the effective EoS parameters are the same for models I, II and III, when $\mathbf{n} = 0$'s go to zero. Hence, in this case the diagrams for $w^{(\text{eff})}$ and q are not redrawn in model(s) II (and III in the later subsection). We arrange the diagrams the same as model I, however in this case the parameter α increases horizontally. An increase in the value of α leads to a decrease in the value of $w_0^{(\text{eff})}$, and this is clearly evident for the relatively smaller values of K . In this model we obtain more acceptable results in all range $0 < \alpha < 1$; upper left diagram shows that even for $\alpha = 0.001$ we have $w_0^{(\text{eff})} \simeq -0.9$ (red dot-dashed line), the result that met in model I only for $K \rightarrow 1$. By comparing the effective EoS diagrams between model I and II we see that the value of $w_0^{(\text{eff})}$ decreases when the value of α increases, and this means that we can construct more acceptable models for larger values of α . In Fig. 5, the related diagrams of the deceleration parameter $q = q(a; \alpha, K, \mathbf{m}, \mathbf{n}^{(\text{II})})$, for $\mathbf{m} = 0, -1, \mathbf{n}^{(\text{II})} = -1$ and $\alpha, K > 0$ are drawn. In the lateral view, the diagrams for the same values of parameters $\mathbf{m}, \mathbf{n}^{(\text{II})}$ for two values $\alpha = 0.01, 0.99$ are pictured. In the columnar view, the plots are arranged for the same value of α and different values of \mathbf{m} . The present value of the deceleration parameter q_0 is displayed in each plot, which can be calculated as

$$q_0^{(\text{II})} = -1 + \frac{3}{4} \left[\Omega_0^{(\text{b})}(2 - \mathbf{m}) + \frac{2(1 - K)(1 + \Omega_0^{(\text{b})})(\mathbf{m} - 1)(1 + \sqrt{27}K^{3/2}\alpha\mathbf{n}^{(\text{II})})}{1 - \sqrt{12}K^{3/2}\mathbf{n}^{(\text{II})}} \right], \quad N = 0, \quad (63)$$

and for the special case $\mathbf{n}^{(\text{II})} = 0$ it can be rewritten as

$$q_0^{(\text{II})} = \frac{3}{4}\Omega_0^{(\text{b})}(1 - 2K)\mathbf{m} + \frac{1}{2}\left(1 - 3K(1 + \Omega_0^{(\text{b})})\right), \quad N = 0, \quad \mathbf{n}^{(\text{II})} = 0. \quad (64)$$

It is obvious that the value of q_0 does not depend on α for the models with $\mathbf{n}^{(\text{II})} = 0$, (that is we have $q_0^{(\text{I})} = q_0^{(\text{II})} = q_0^{(\text{III})}$ for \mathbf{n} 's = 0). The related plots for $\mathbf{n}^{(\text{II})} \neq 0$ are presented in the first row of Fig. 5. As the plots show, for the cases with $\mathbf{n}^{(\text{II})} \neq 0$ an increase in the value of α results in a decrease in the value of q_0 . The models with observationally inconsistent value of q_0 can be put in an acceptable regime (for which we have $q_0 \simeq -0.6$) by choosing a value for parameter $\mathbf{n}^{(\text{II})}$, properly. This arbitrariness can not be met in GR regime,

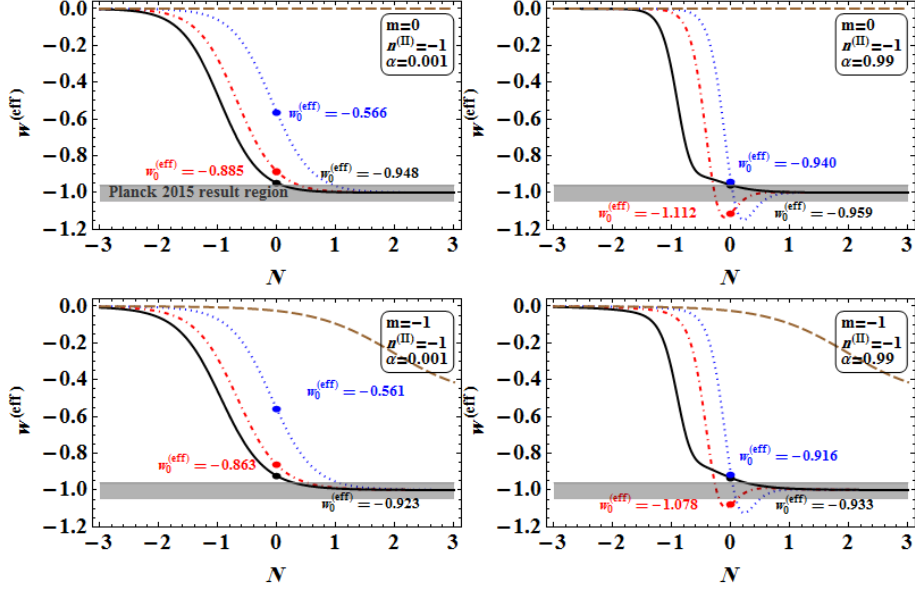


Figure 4: (color online). The evolution of the effective EoS parameter for model II which uses the non-interacting baryonic matter together with GCG in the high pressure regime. The curves are plotted for $K = 0$ (brown dashed line), $K = 0.33$ (blue dotted line), $K = 0.77$ (red dot-dashed line) and $K = 0.99$ (black solid line), for $\mathbf{m} = 0, -1$, $\mathbf{n}^{(\text{II})} = -1$ and $\alpha = 0.001, 0.99$. The present values are also depicted with the corresponding colors. The valid range of values reported by Planck 2015 measurements, $(-1.051 \leq w_{0,\text{Planck}}^{(\text{eff})} \leq -0.961)$ is indicated by the gray region. An increase in the value of α , leads to a decrease in the value of $w_0^{(\text{eff})}$.

where $f(R, T) = R$. In GR, observationally consistent values can be achieved only for $K \simeq 1$, irrespective of the value of α . However in $f(R, T)$ gravity one can attain the consistent Chaplygin gas models with arbitrary value of K only by a suitable choice of the coupling constant $\mathbf{n}^{(\text{II})}$, (compare the diagrams in the top panels in Fig. 2 with the diagrams in Fig. 5). Comparing the first row with the second one in Fig. 5, shows that turning parameter \mathbf{m} on increases the values of the deceleration parameter. Equation (63) shows that the present value of the deceleration (and also the effective EoS) parameter for $\mathbf{n}^{(\text{II})} = -1$ is not as simple as the result given in (64), and therefore the effect of variation of \mathbf{m} is not obvious for each value of K . However, as diagrams in Fig. 5 show, decreasing the value of \mathbf{m} increases the value of q_0 . Comparing the diagrams for model I in Fig. 2 with the diagrams in Fig. 5, one can find more acceptable results in model II for large values of α .

In Fig 6 we have depicted (r, s) plane diagrams for different values $K = 0.33, 0.77, 0.99$, $\mathbf{m}, \mathbf{n}^{(\text{II})} = 0, -1$ and $\alpha = 0.001, 0.99$. These diagrams have been arranged in such a way that the parameter α varies in the horizontal view and the coupling constants $\mathbf{m}, \mathbf{n}^{(\text{II})}$ in the vertical view. Comparison of the lateral

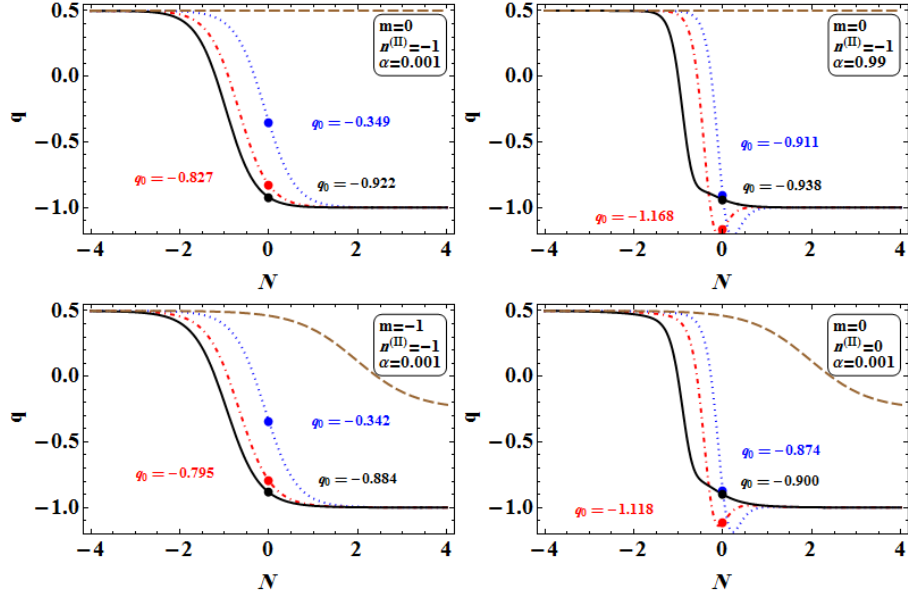


Figure 5: (color online). The evolution of the deceleration parameter for type II models for different values of the parameters K , $\mathbf{m} = 0, -1$ and $\mathbf{n}^{(\text{II})} = -1$. The curves are plotted for $K = 0$, $K = 0.33$, $K = 0.77$ and $K = 0.99$, corresponding to brown dashed line, blue dotted line for, red dot-dashed line and black solid line. In this case, a lateral view shows that the value of the deceleration parameter decreases when parameter α increases. And, a vertical view shows that decreasing \mathbf{m} , results in increasing the value of q_0 .

diagrams shows that in the high pressure regime a growth in the value of α would result in a decrease in the value of s_0 and increases the value of r_0 for $\mathbf{n}^{(\text{II})} = 0$. However, when $\mathbf{n}^{(\text{II})} < 0$ this feature cannot be seen for large values of K . This means that the distance to the Λ CDM fixed point becomes so long when α approaches to 1 and k gets away from 1. That is, the models with large values of α and small values of K are distinguishable from the Λ CDM model in the high pressure regime. However, since the Λ CDM is the mostly accepted cosmological model, these models cannot be very interesting. The upper left panel holds for GR regime which resembles the Λ CDM model, since, we have $s_0 \propto -10^{-3}$ and $r_0 \approx 1$. In the vertical view, we see that decreasing the values of \mathbf{m} does not lead to a significant variations of the parameters r_0 and s_0 . Therefore, decreasing in the value of \mathbf{m} does not affect the distance of underlying model. Furthermore, when $\mathbf{n}^{(\text{II})}$ decreases, the present fixed point (s_0, r_0) gets farther from the Λ CDM one only for large values of α and small values of K .

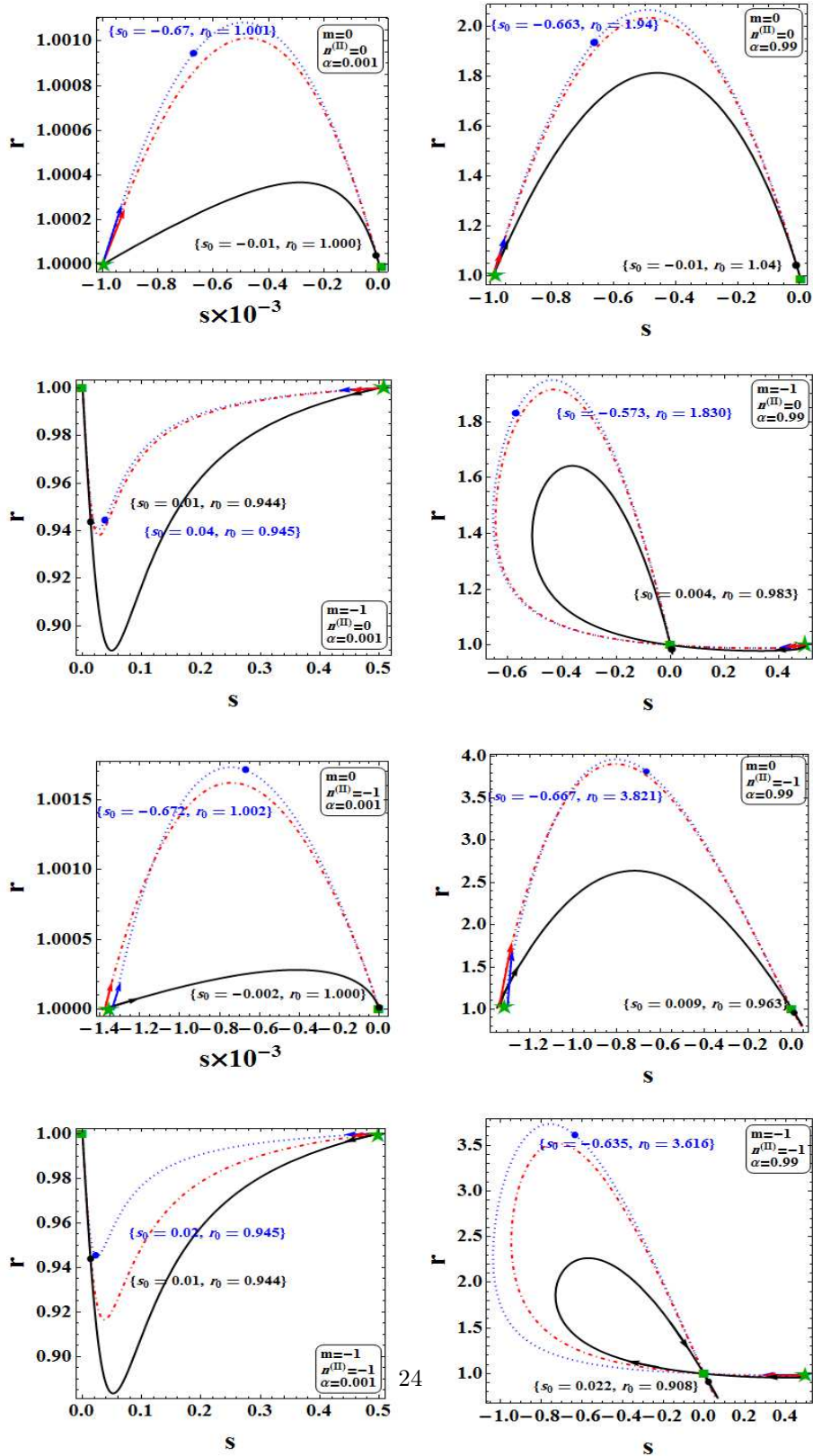


Figure 6: (color online). Cosmological trajectories of model II in the (s, r) plane. The plots show that an increase in the value of α , has a significant effect on the values of statefinder parameters for smaller values of K , and accordingly, these models have a distinct situation with respect to the Λ CDM model.

4.3 model $f^{(\text{III})}(R, T^{(\text{b}), \mathbf{G}})$

This case differs from model II only when $\mathbf{n}^{(\text{III})} \neq 0$. Both models II and III have the same behavior for $\mathbf{n}^{(\text{II})} = \mathbf{n}^{(\text{III})} = 0$. The other important point about model III is that, the present values of the deceleration parameter q_0 and therefore w_0 , are independent of the values of α for arbitrary values of $\mathbf{n}^{(\text{III})}$. The present value of the deceleration parameter for this model reads

$$q_0^{(\text{III})} = \frac{3}{4(1 - 2\mathbf{n}^{(\text{III})})} \left[\Omega_0^{(\text{b})} (1 - 2K(1 - \mathbf{n}^{(\text{III})})) \mathbf{m} - 2 \left(K(\Omega_0^{(\text{b})} - 1) + 2\Omega_0^{(\text{b})} + 1 \right) \mathbf{n}^{(\text{III})} + 2 \left(K(\Omega_0^{(\text{b})} - 1) + 1 \right) \right], \quad N = 0, \quad (65)$$

whence we observe that the parameter α does not play any role in the value of $q_0^{(\text{III})}$. In Fig 7 and Fig 8 we present the related diagrams of the effective EoS and the deceleration parameters for $\mathbf{n}^{(\text{III})} = -1$, $\mathbf{m} = 0, -1$, respectively. By indicating the parameter α on diagrams, we emphasize that the present values do not depend on α . when parameter \mathbf{m} is switched on, an increase in the

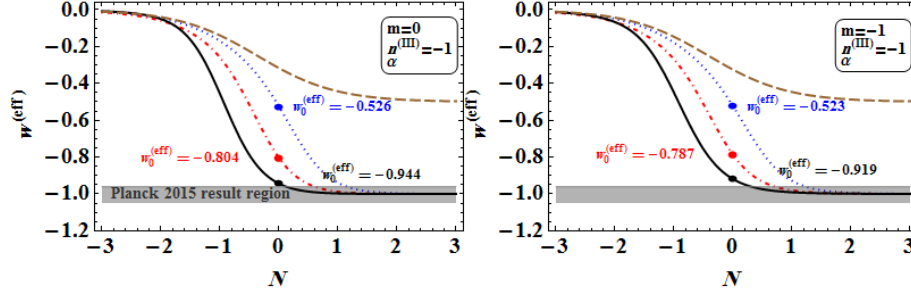


Figure 7: (color online). The evolution of the EoS parameter for model III. Here the values of α has no effect on the values of $w^{(\text{eff})}$.

values of w_0 and q_0 would happen. Such an effect appears in model II, as well. Since, when \mathbf{n} 's= 0, we have the same values of w_0 and q_0 for the three models, therefore to understand the effect of decreasing the value of $\mathbf{n}^{(\text{III})}$ from zero to an arbitrary negative value (here -1), one can compare the diagrams of Fig. 8 (or Fig. 7 for the EoS parameter of model III) with the corresponding ones in Fig. 2 (or Fig. 1 for the EoS parameter of model I). We see that decreasing ones in the values of $\mathbf{n}^{(\text{III})}$ would reduce the values of q_0 and w_0 , and the net effect is more significant for smaller values of K . Thus, again decreasing $\mathbf{n}^{(\text{III})}$ to negative values can help to construct more reliable models with admissible values of w_0 and q_0 . In Figure 9 we present the related diagrams for the statefinder parameters of model III. These diagrams are plotted for $\mathbf{n}^{(\text{III})} = -1$, since the diagrams for $\mathbf{n}^{(\text{III})} = 0$ are the same as the diagrams for model II with $\mathbf{n}^{(\text{II})} = 0$. Comparing the plots of Fig. 9 with four upper diagram in Fig. 6 indicates that

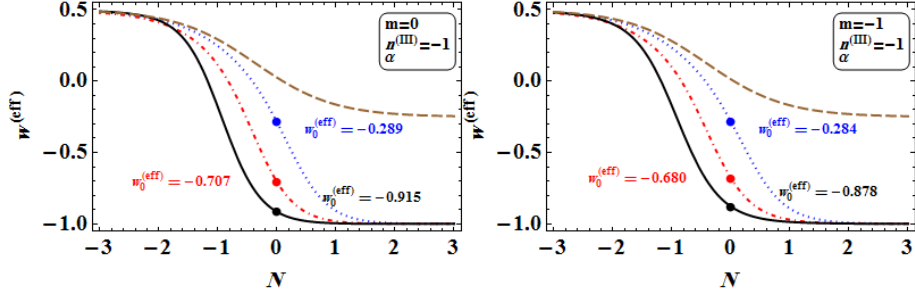


Figure 8: (color online). The evolution of the deceleration parameter for model III. The values of q_0 are independent of the values of α .

a decrease in the value of $\mathbf{n}^{(\text{III})}$ makes the distance of model III to the Λ CDM model shorter for large values of α and longer for small values of this parameter. As diagrams of Fig. 9 show, an increase in the value of α , decreases the value of s_0 and makes r_0 to get larger values. The overall behavior of this, is to lengthen the distance to the Λ CDM fixed point. Nevertheless, the effect is weak for larger values of K . A vertical view indicates that decreasing the parameter \mathbf{m} , has no remarkable effect on the present values of the statefinder parameters, though it leads the distance to become slightly shorter for larger values of α and smaller value of K .

5 Luminosity distance and Hubble parameter tests

So far we have discussed the $f(R, T)$ cosmological solutions when a generalized Chaplygin gas along with a baryonic matter are present as the whole matter content. We have obtained three different forms for $f(R, T)$ function based on the EMT conservation and subsequently the cosmological consequences of these models have been extracted from a theoretical point of view. In this section, these solutions will be compared to SNIa cosmological data and the compilation of Hubble parameter measurements. Supernovae type Ia as accurate standard candles are the most direct probe to detect signatures of the accelerated expansion of the Universe as well as DE. Therefore, Dark energy scenarios in the first step can be examined by comparing their predicted luminosity distance to the observational data. In this regard, we apply the chi-square test of the goodness of fit of the Hubble parameter and modulus distance quantity defined by equations (42)-(44) for models I, II and III to the observational data. The procedure of fitting can be summarized as follows: The supernova observations include N apparent magnitude m_i which can be translated to a quantity which is called "distance modulus μ_i ", the corresponding redshift z_i and their errors.

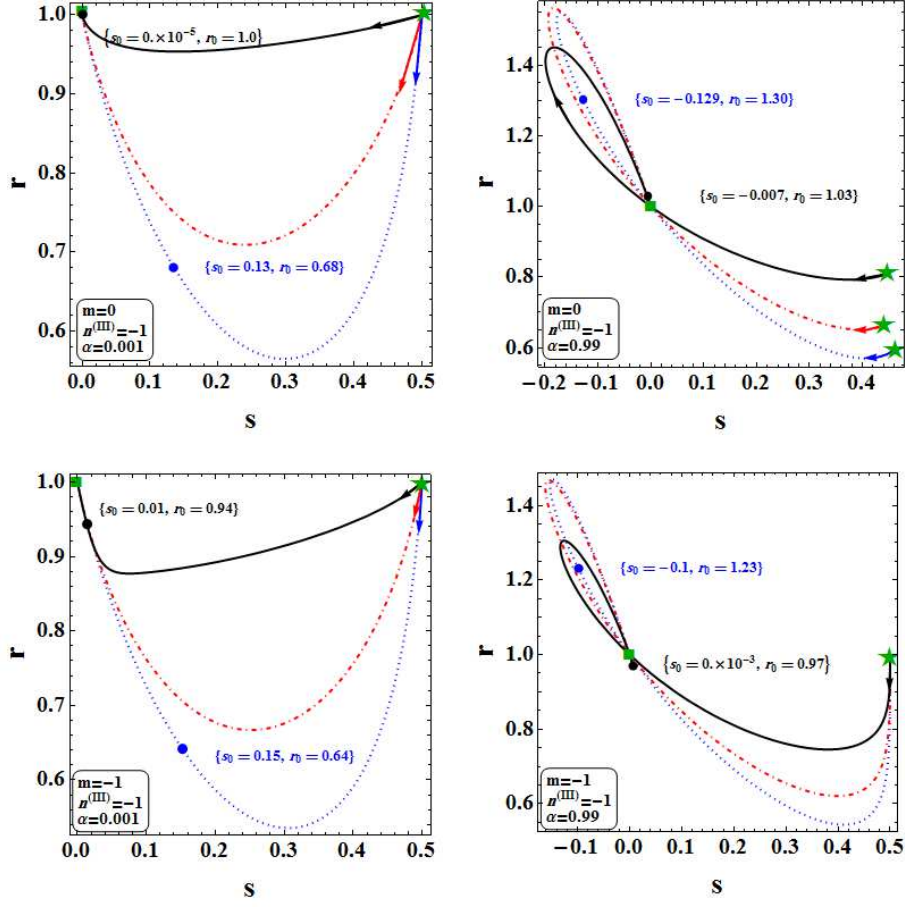


Figure 9: (color online). Statefinder diagnosis of model III in the (s, r) plane. Only the diagrams for $\mathbf{n}^{(\text{III})} = -1$ are plotted since the case $\mathbf{n}^{(\text{III})} = 0$ is the same as the results of model II when $\mathbf{n}^{(\text{II})} = 0$. Horizontal view shows that if the value of α increases, the distance to the Λ CDM fixed point will slightly enlarge. Also, a decrease in the value of \mathbf{m} has no effective impact on the present values.

Theoretically, these quantities satisfy the following equation

$$\mu(z) \equiv m(z) - M = 25 + 5 \log \left(\frac{d_L(z)}{1 \text{Mpc}} \right), \quad (66)$$

where the luminosity distance d_L is defined as

$$d_L(z) = \frac{c}{H_0} (1+z) \int_0^z \frac{dz'}{H(z')}. \quad (67)$$

Generally, for a given model, the Hubble parameter $H(z)$ can be written as a function of some parameters like those presented in our cases. For example, we have $H(z; \mathbf{m}, \mathbf{n}'s, K, \alpha)$ in this paper. The idea is to find the best fit values of the model parameters which lead to the most consistency between the predicted curves of the modulus distance as well as the Hubble parameter (by the virtue of the underlying theoretical model) and the observational data. To this aim, we minimize the quantities

$$\chi_\mu^2(\mathbf{m}, \mathbf{n}'s, K, \alpha) = \sum_{i=1}^N \frac{[\mu^{(o)}(z_i) - \mu^{(\text{th})}(z_i)]^2}{\sigma_{\text{H},i}^2 - \sigma_{\text{mz},i}^2}, \quad (68)$$

and

$$\chi_{\text{H}}^2(\mathbf{m}, \mathbf{n}'s, K, \alpha) = \sum_{j=1}^{N'} \frac{[H^{(o)}(z_j) - H^{(\text{th})}(z_j)]^2}{\sigma_{\mu,j}^2}, \quad (69)$$

where $\mu^{(o)}(z_i)$ and $H^{(o)}(z_i)$ are obtained from observations, $\mu^{(\text{th})}(z_i) = \mu^{(\text{th})}(z_i; \mathbf{m}, \mathbf{n}'s, K, \alpha)$ and $H^{(\text{th})}(z_i) = H^{(\text{th})}(z_i; \mathbf{m}, \mathbf{n}'s, K, \alpha)$ denotes the distance modulus and the Hubble parameter predicted by theory, z_i is the redshift of an event obtained from observation, $\sigma_{\mu,i}$ and $\sigma_{\text{H},i}$ are the errors caused by measurement and $\sigma_{\text{mz},i}$ is dispersion in the distance modulus. There are some packages on the web that can help one to minimize the chi-square function for the best fit parameters of theory. For example, in [134] one can find the self-study package ‘‘CoChiSquare alpha’’ which is written in both Mathematica [135] and Python [136] languages, or the one which is released in [137]. After minimizing the chi-square parameter for the best fit values, if $\chi_{\text{min}}^2(\overline{\mathbf{m}}, \overline{\mathbf{n}'s}, \overline{K}, \overline{\alpha})/d.o.f \lesssim 1$ then we have a good fitting and the theory is consistent with the data. ‘‘d.o.f’’ stands for the number of degrees of freedom which is equal to $N - n$ in which N is the total number of measurements, n is the number of parameters of theory, and the barred parameters in the argument are the best fit values.

In our study we have used the Union 2 sample which consists of 557 type Ia supernova data [124] as well as 28 Hubble parameter measurements⁹ which are collected in Ref. [125]. We minimize the chi-square function to find the best fit values of \mathbf{m} , $\mathbf{n}'s$, K and α parameters for the fixed values $H_0 = 67.8$

⁹The original data can be found in Refs.[126, 127, 128, 129, 130, 131, 132, 133]

$kms^{-1}Mpc^{-1}$, $\Omega_0^{(b)} = 0.05$ and $c = 2.99 \times 10^8 ms^{-1}$. The results are summarized in Table 1. In this table in addition to $\chi_{(\mu, H) \min}^2$ and $\chi_{(\mu, H) \min}^2/d.o.f$ the effective EoS and the value of deceleration parameter for the best fit values of model parameters (which are obtained in the modulus distance and Hubble chi-square tests) are shown. As shown in Table 1, these best fit values for modulus distance test would result in a good consequence both for models I and II. We have obtained $\chi_{\mu, min}^2/d.o.f \simeq 1.0073$ for model I and $\chi_{\mu, min}^2/d.o.f \simeq 1.0104$ for model II, which show a relatively good consistency of these models with the SNIa observations. In these cases, the best fit values give an acceptable present value for the effective EoS. Nevertheless, the best fit values in the Hubble chi-square tests do not lead to a satisfactory result for $w^{(eff)}$ in both cases. The diagrams of the modulus distance along with the Union 2 sample data, the effective EoS and the Hubble parameter along with the related observational data [125] for models I and II are drawn in Fig. 10 and Fig. 11, respectively. These figures are drawn for $K_\mu = 0.210$, $m_\mu = 15$ and $n_\mu^{(I)} = -2.2$ in model I and $K_\mu = 0.295$, $m_\mu = 6.1$, $n_\mu^{(II)} = -2.34$, $\alpha_\mu = 0.34$ in model II which minimize the modulus distance chi-square parameter. As is seen, they show a relatively consistent behavior, at least in low redshifts.

Table 1 also gives the present values of the statefinder parameters s_0 and r_0 which are calculated for the best fit values of parameters for models I, II and III. In comparison to the results of the gold sample supernova type Ia which gives $1.65 < r_0^{(Gold)} < 3.97$ and $-0.86 < s_0^{(Gold)} < -0.13$ [92], the SNLS supernova type Ia data set which results in $0.11 < r_0^{(SNLS)} < 2.69$ and $-0.61 < s_0^{(SNLS)} < 0.32$ [93] and X-ray galaxy clusters analysis with $-1.49 < r_0^{(X-ray)} < 3.06$ and $-0.56 < s_0^{(X-ray)} < -0.094$ [94], we see that model II, namely, $f(R, T)$ gravity with GCG in high pressure regime shows a good consistency with these data. Only, model II (for the best fit values of parameters which minimize the modulus distance chi-square) is approximately consistent with all these three data sets.

Similar considerations can be done for model III in search of the observationally acceptable model parameters. Nevertheless, we will report the results of a full statistical discussion on these models, elsewhere. The most performed cosmological tests in the literature consist of the luminosity distance tests, experiments on cosmic microwave background radiation (CMB), the baryon acoustic oscillation (BAO) probes, investigations about look-back time and the age of the Universe and the growth rate of matter density perturbations.

We conclude this section by commenting that, the model of the Chaplygin gas in the framework of $f(R, T)$ gravity can deserve further investigations. Some research works have treated this issue [95, 96, 97, 98, 99, 100], where it is shown that the standard Chaplygin gas in the background of GR may not be consistent with observations, however, here we have demonstrated that this type of matter can be survived, still in $f(R, T)$ modified theory of gravity. Although, using more precise statistical techniques for different cosmological tests can give better results.

Table 1: Results of the modulus distance and Hubble chi-square tests for models I, II and III.

Models	$\chi_{(\mu,H)}^2 \min$	$\chi_{(\mu,H)}^2 \min/d.o.f$	Best fit values of the model parameters	q_0	$w_0^{(\text{eff})}$	s_0	r_0
Model I	20.667	0.827	$K_H = 0.180, m_H = -7.68, n_H^{(\text{I})} = -4.66, \alpha - - - -$	-0.604	-0.736	-0.12	1.4
Model I	558.024	1.0073	$K_\mu = 0.210, m_\mu = 15, n_\mu^{(\text{I})} = -2.2, \alpha - - - -$	-1.01	-1.008	-0.65	3.97
Model II	23.680	0.947	$K_H = 0.35, m_H = -7.10, n_H^{(\text{II})} = -2.56, \alpha_H = -0.33$	-0.267	-0.511	0.31	0.28
Model II	558.774	1.0104	$K_\mu = 0.295, m_\mu = 6.1, n_\mu^{(\text{II})} = -2.34, \alpha_\mu = 0.34$	-0.978	-0.967	-0.37	2.62
Model III	552.612	0.9993	$K_\mu = 0.280, m_\mu = 1.0, n_\mu^{(\text{III})} = -1.5, \alpha_\mu = 0.28$	-0.552	-0.288	0.09	0.77

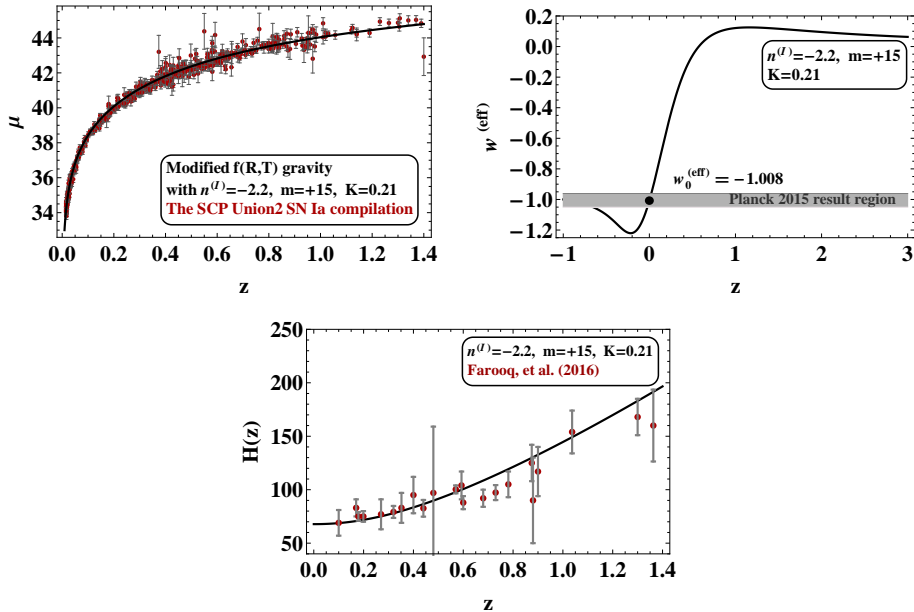


Figure 10: (color online). Cosmological diagrams for the best fit values of model I parameters obtained from the modulus distance chi-square test. The upper left panel shows the modulus distance and the Union 2 compilation data which are shown in red points. The upper right panel presents the effective EoS parameter. In this plot the valid range of values reported by Planck 2015 measurements ($-1.051 \leq w_{0,\text{Planck}}^{(\text{eff})} \leq -0.961$) is indicated by the gray region. The lower one depicts the Hubble parameter along with the Hubble cosmological data which is illustrated in red color.

6 conclusions

In the present work we have investigated cosmological behavior of the generalized Chaplygin gas (GCG) in $f(R, T)$ theory of gravity endowed with a homogeneous and isotropic FLRW spacetime, by means of statefinder diagnosis. More precisely, the baryonic matter is also included which does not directly interact with GCG. However, these two fluids interact with each other via a non-standard geometric rule which is imposed by $f(R, T)$ gravity Lagrangian. Here, the coupling of the trace of whole matter to geometry would relate the evolution of these two type of matters to each other.

In $f(R, T)$ gravity conservation of energy-momentum tensor (EMT) enforces us to use a constraint equation which must hold by $f(R, T)$ function. This equation gives the functionality of R and T by the virtue of which the conservation of EMT is guaranteed. Only models of type $f(R, T) = g(R) + h(T)$ respect the EMT conservation. However, we have worked on the special case $f(R, T) = R + h(T)$, although models $f(R, T) = g(R) + h(T)$ are worthy of study as well. Adding a matter trace dependent term to the Ricci scalar can be accounted for as a correction to the Einstein-Hilbert action. We solved the con-

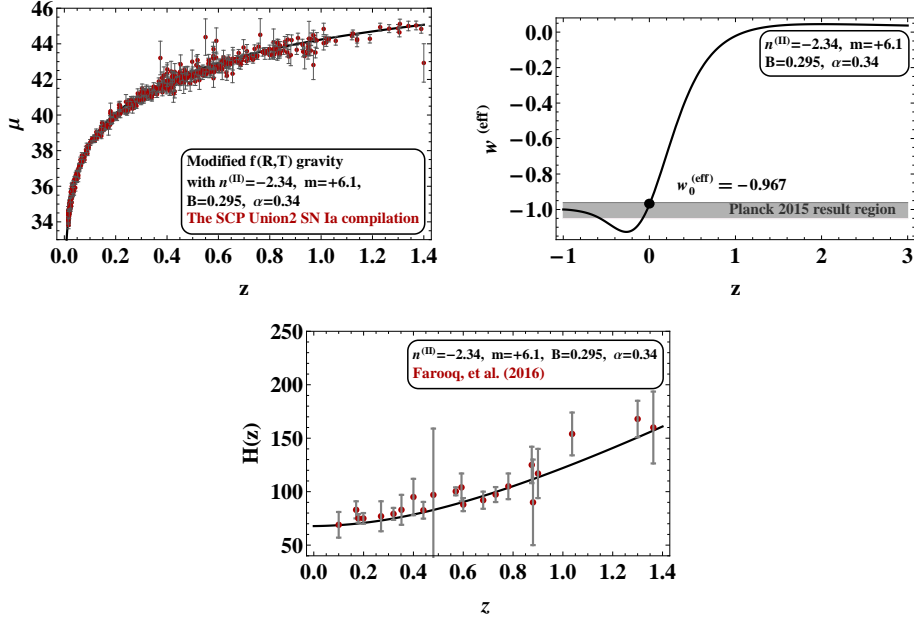


Figure 11: (color online). Cosmological diagrams for the best fit values of model II parameters obtained from the modulus distance chi-square test.

straint equation for two class of models; the models that employ the standard Chaplygin gas (SCG) and those that make use of GCG. All related equations (specially the function $f(R, T)$) of the former are exactly obtained. Nevertheless, the constraint equation can not be exactly solved for the latter because of the appearance of constant α in the GCG sector. In fact, for each value of this constant (which may be whether integer or not) there may be numerous solutions so that dealing with them is time consuming. To avoid such mathematical problems we approximate the constraint equation in two extreme limits, the high pressure ($p \gg \rho$) and the high density regimes ($\rho \gg p$). Of course, we have supposed that under these two extreme situations, the Chaplygin gas preserves its nature. As a result, we have mainly worked on three classes of Chaplygin gas models; the models in which SCG is included and we classified them as model I, the GCG models in the high pressure regime, as models II and finally the GCG models in the high density regime as models III.

After obtaining and then normalizing the Hubble parameter for each model, we obtained the deceleration and the statefinder parameters, from which one can differentiate these models from DE point of view. The statefinder diagnosis is a powerful tool to understand the behavior of different DE scenarios. In our models, there are some parameters that enable us to choose the best values for them in order to make the models consistent with the observational results. Model I contains parameter \mathbf{m} which is related to the coefficient of the baryonic term in the $f(R, T)$ function, $\mathbf{n}^{(I)}$ which corresponds to the SCG term in the

$f(R, T)$ function and K which is included in the SCG density. In addition to parameters $\mathbf{n}^{(\text{II})}$ and $\mathbf{n}^{(\text{III})}$ which correspond to the GCG terms in the $f(R, T)$ functions and constant K that comes from GCG density, we have constant α for the two other models. In our work, we have used different values for these parameters and have plotted various diagrams for the effective EoS, the deceleration parameter and the statefinder parameters which all are calculated from the modified normalized Hubble parameter for each model. Note that, we have used the present value for the baryonic density parameter which is about five percent of the total matter density parameter. In each diagram we have indicated the present values of the related quantities in order to compare the predictions of the underlying model with the corresponding observational values. Particularly, we have plotted the curves of quantities which hold in the GR background (i.e. when the constants \mathbf{m} and \mathbf{n} 's do vanish) in order to compare them with the $f(R, T)$ corresponding plots and have investigated the possible deviations. We mentioned that positive values for parameters \mathbf{m} and \mathbf{n} 's lead to some divergences in diagrams and consequently to non-physical outcomes. As a result, we have not followed our considerations for positive values of these parameters. The effective EoS parameter for our models starts from a zero value in the early stages of the evolution of the Universe and converges to -1 , as is expected. Note that the models of GCG/SCG in the GR background show a similar behavior [114] (as we also depicted this behavior in the diagrams). However, in $f(R, T)$ gravity the present values can be improved as compared with the corresponding GR ones. As we have shown, in the GR background, only for cases with $K \rightarrow 1$ we have $w_0^{(\text{eff})} \simeq -1$. Nevertheless, in $f(R, T)$ gravity this value will improve. For example, the values of the EoS parameter for $K = 0.33$ is $w_0^{(\text{eff})(\text{GR})} \simeq -0.314$ and the corresponding values in the three models are; $w_0^{(\text{eff})(\text{I})} \simeq -0.773$ for $\mathbf{m} = 0$ and $\mathbf{n}^{(\text{I})} = -1$, $w_0^{(\text{eff})(\text{II})} \simeq -0.916$ for $\mathbf{m} = -1$, $\mathbf{n}^{(\text{II})} = -1$ and $\alpha = 0.99$, and $w_0^{(\text{eff})(\text{III})} \simeq -0.526$ for $\mathbf{m} = 0$, $\mathbf{n}^{(\text{III})} = -1$ and an arbitrary constant α . Comparing these values we get another important point. For models I and III, the best values are obtained for $\mathbf{m} = 0$, which means the baryonic term is absent. It shows that in these models the pure SCG/GCG can drive the accelerated expansion of the Universe in $f(R, T)$ gravity. The better values have obtained in model II, when a mixture of the baryonic matter and the GCG in the high pressure regime are included. Note that, the larger constant K becomes, the more observationally accepted values the EoS parameter gets. It means that models I and III can still be compatible provided that constants K and α are selected properly. However, model II can give admissible values even for smaller values of K . There is a special case; the values of $w_0^{(\text{eff})}$ and q_0 do not remain constant for $K = 0$ when $\mathbf{m} = -1$ in models I and II and arbitrary values of \mathbf{m} for model III, (in this case we must have $w_0^{(\text{eff})} = 0$ and $q_0 = 0.5$). In all models with $K = 0$, CG plays the role of CDM and therefore DE is absent in the history of the evolution of the Universe. However, in $f(R, T)$ gravity, the mixture of DM and the baryonic matter can lead to the accelerated expansion.

Also, we have investigated these three Chaplygin gas models in (s, r) plane, where s and r are the statefinder parameters. This tool would allow us to

discriminate between different models of DE. In the statefinder diagnosis, the difference between the predicted present values s_0 and r_0 of the models and the corresponding values for Λ CDM model (which is called the distance to the Λ CDM model) is used as a criteria for discrimination of DE models. Note that, we have $s^{(\Lambda\text{CDM})} = 0$ and $r^{(\Lambda\text{CDM})} = 1$, which this fixed point is indicated by a green solid box in our diagrams. We have derived these parameters for the three models and have plotted their evolutionary trajectories for different values of K , \mathbf{m} , \mathbf{n} 's and α . For the sake of clarity, we have also drawn the GR corresponding results. In model I, the distance to the Λ CDM model becomes shorter as compared with the same model with the GR background. For $\mathbf{m} = -1$ and $\mathbf{n}^{(\text{I})} = 0$ both statefinder parameters slightly approach to the corresponding values for Λ CDM model, and the minimum distance achieved when both \mathbf{m} and $\mathbf{n}^{(\text{I})}$ get negative values. Moreover, we have shorter distances for larger values of K , for all values of \mathbf{m} and $\mathbf{n}^{(\text{I})}$. The models of class I, can be categorized in two different subclasses based on the initial values of the statefinder parameter s ; some models have trajectories starting from $s = -1/2$ which correspond to $\mathbf{m} = 0$. However, trajectories of some other models start from $s = +1/2$ with negative values of \mathbf{m} . Within the models which belong to class II, there are several possibilities that can be considered as different scenarios of DE and can be classified in three different categories based on their values of the statefinder parameters:

- (i) There are Chaplygin gas models that are not effectively distinguishable from the Λ CDM model. They have $|s^{(\text{II})} - s^{(\Lambda\text{CDM})}|, |r^{(\text{II})} - r^{(\Lambda\text{CDM})}| \lesssim 10^{-3}$, corresponding to $\alpha \ll 1$.
- (ii) Models that have long distance from the Λ CDM model, and they appear when $\mathbf{n}^{(\text{I})} < 0$ and $\alpha \rightarrow 1$.
- (iii) The models that can be accounted for the third category and include large values of α . Their distance are between those of categories (i) and (ii).

Note that, all cases with $K \rightarrow 1$ have shorter distance than other ones. In class III of models all trajectories start from $s = 1/2$ in the (s, r) plane. The distance to the Λ CDM model is weakly affected by variation of the value α when $\mathbf{n}^{(\text{III})} < 0$. For $\mathbf{n}^{(\text{III})} = 0$, the trajectories are the same as those models of class II and belong to categories (i) and (iii). Finally, we have employed the chi-square test to examine models I, II and III using recent observational data. Specifically, the Union 2 sample including 557 SNIa data and 28 Hubble parameter measurements have been used and the best fit values of the model parameters by minimizing the so called chi-square function (it can be accounted for as the function of all model parameters) have been obtained. We found that in models I and II, the behavior of the modulus distance, the Hubble parameter and the effective EoS parameter are consistent with the observations for those best fit parameters which minimize the modulus distance chi-square. In this case we have obtained $\chi_{\mu, \min}^{2, (\text{I})}/d.o.f = 1.0073$ and $\chi_{\mu, \min}^{2, (\text{II})}/d.o.f = 1.0104$

which show admissible values. The best fit parameters gained from the Hubble parameter chi-square test lead to a non-compatible value for the present effective EoS parameter and also in this case the theoretical curve of modulus distance does not match the observational data in both models I and II. We compared the values of statefinder parameters which are predicted by these three models by the observational data. It is shown that the results from the observational constraints on the statefinder parameters are in favor of model II. We came to conclusion that the results of performed studies in this work, for $f(R, T)$ gravity with GCG in high pressure regimes can be reassuring enough to merit further investigations.

Acknowledgments

The author acknowledges the university of Sistan and Bluchestan for financial support, Grant No. 2016-952/2/348 and also is grateful to Amir Hadi Ziaie for helpful discussions and correspondence.

References

- [1] Riess, A.G., *et al.* "Observational evidence from supernovae from an accelerating universe and a cosmological constant", *Astron. J.* **116** (1998), 1009.
- [2] Perlmutter, S., *et al.* (The Supernova Cosmology Project), "Measurements of Ω and Λ from 42 high-redshift supernovae", *Astrophys. J.* **517** (1999), 565.
- [3] Riess, A.G., *et al.* "BVRI curves for 22 type Ia supernovae", *Astron. J.* **117** (1999), 707.
- [4] Spergel, D.N., *et al.* "First year wilkinson microwave anisotropy probe (WMAP) observations: determination of cosmological parameters", *Astrophys. J. Suppl.* **148** (2003), 175.
- [5] Tegmark, M., *et al.* "Cosmological parameters from SDSS and WMAP", *Phys. Rev. D* **69** (2004), 103501.
- [6] Abazajian, K., *et al.* "The second data release of the Sloan Digital Sky Survey", *Astron. J.* **128** (2004), 502.
- [7] Abazajian, K., *et al.* "The third data release of the Sloan Digital Sky Survey", *Astron. J.* **129** (2005), 1755.
- [8] Spergel, D.N., *et al.* "Wilkinson microwave anisotropy probe (WMAP) three year results: implications for cosmology", *Astrophys. J. Suppl.* **170** (2007), 377.

- [9] Komatsu, E, *et al.* "Five-Year wilkinson microwave anisotropy probe (WMAP) observations: cosmological interpretation", *Astrophys. J. Suppl.* **180** (2009) ,330.
- [10] Komatsu, E, *et al.* "Seven-Year wilkinson microwave anisotropy probe (WMAP) observations: cosmological interpretation", *Astrophys. J. Suppl.* **192** (2011) ,18.
- [11] Hinshaw, G.F., *et al.* "Nine-Year wilkinson microwave anisotropy probe (WMAP) observations: cosmological parameter results", *Astrophys. J. Suppl.* **208** (2013) ,19.
- [12] Bertonea, G., Hooperb, D. & Silk, J. "Particle dark matter: evidence, candidates and constraints", *Phys. Rep.* **405** (2005), 279.
- [13] Silk, J. "Dark matter and galaxy formation", *Ann. Phys. (Berlin)* **15** (2006), 75.
- [14] Feng, J.L. "Dark matter candidates from particle physics and methods of detection", *Annu. Rev. Astron. Astrophys.* **48** (2010), 495.
- [15] Bergström, L. "Dark matter evidence, particle physics candidates and detection methods", *Ann. Phys. (Berlin)* **524** (2012), 479.
- [16] Frenk, C.S. & White, S.D.M. "Dark matter and cosmic structure", *Ann. Phys. (Berlin)* **524** (2012), 507.
- [17] Destri, C., de Vega, H.J., & Sanchez, N.G. "Warm dark matter primordial spectra and the onset of structure formation at redshift z", *Phys. Rev. D* **88** (2013), 083512.
- [18] Cheng, D., Chu, M.-C. & Tang, J. "Cosmological structure formation in decaying dark matter models", *J. Cosmol. Astropart. Phys.* **07** (2015), 009.
- [19] Vogelsberger, M. *et al.* "ETHOS - An effective theory of structure formation: dark matter physics as a possible explanation of the small-scale CDM problems", *Mon. Not. R. Astron. Soc.* **460**, (2016), 1399.
- [20] Peebles, P.J.E. "The cosmological constant and dark energy", *Rev. Mod. Phys.* **75** (2003), 559.
- [21] Polarski, D. "Dark energy: current issues", *Ann. Phys. (Berlin)* **15** (2006), 342.
- [22] Copeland, E.J., Sami, M. & Tsujikawa, S. "Dynamics of dark energy", *Int. J. Mod. Phys. D* **15** (2006), 1753.
- [23] Durrer, R. & Maartens, R. "Dark energy and dark gravity: theory overview", *Gen. Rel. Grav.* **40** (2008), 301.

- [24] Rosales, J.J. & Tkach, V.I. "Supersymmetric cosmological FRW model and dark energy", *Phys. Rev. D* **82** (2010), 107502.
- [25] He, J.-H., Wang, B. & Abdalla, E. "Testing the interaction between dark energy and dark matter via latest observations", *Phys. Rev. D* **83** (2011), 063515.
- [26] Xia, J.-Q. "New limits on coupled dark energy from Planck", *J. Cosmol. Astropart. Phys.* **11** (2013), 022.
- [27] Yang, W. & Xu, L. "Coupled dark energy with perturbed Hubble expansion rate", *Phys. Rev. D* **90** (2014), 083532.
- [28] Linde, A., Roest, D. & Scalisi, M. "Inflation and Dark Energy with a Single Superfield", *J. Cosmol. Astropart. Phys.* **03** (2015), 017.
- [29] Odderskov, I., Baldi, M. & Amendo, L. "The effect of interacting dark energy on local measurements of the Hubble constant", *J. Cosmol. Astropart. Phys.* **05** (2016), 035.
- [30] Wang, B., Abdalla, E., Atrio-Barandela, F., Pavon, D. "Dark matter and dark energy interactions: Theoretical challenges, cosmological implications and observational signatures", arXiv:1603.08299 [astro-ph].
- [31] Dodelson, S. *et al.* "Cosmic Visions Dark Energy: Science", arXiv:1604.07626 [astro-ph].
- [32] Ade, P.A.R. *et al.* "Planck 2013 results. XVI. cosmological parameters", *A&A* **571** (2013), A16.
- [33] Ade, P.A.R. *et al.* "Planck 2015 results. XIII. cosmological parameters", *astro-ph/1502.01589*.
- [34] Ostriker, J.P. & Steinhardt, P.J. "Cosmic concordance", *astro-ph/9505066*.
- [35] Weinberg, S. "The cosmological constant problem", *Rev. Mod. Phys.* **61** (1989), 1.
- [36] Nobbenhuis, S. "The cosmological constant problem, an inspiration for new physics", *gr-qc/0609011*.
- [37] Padmanabhan, H. & Padmanabhan, T. "CosMIn: The solution to the cosmological constant problem", *Int. J. Mod. Phys. D* **22** (2013), 1342001.
- [38] Bernard, D. & LeClair, A. "Scrutinizing the cosmological constant problem and a possible resolution", *Phys. Rev. D* **87** (2013), 063010.
- [39] Narimani, A., Afshordi, N. & Scott, D. "How does pressure gravitate? Cosmological constant problem confronts observational cosmology", *J. Cosmol. Astropart. Phys.* **08** (2014), 049.

- [40] Moffat, J.W. "Quantum gravity and the cosmological constant problem", *gr-qc/1407.2086*.
- [41] Padilla, A. "Lectures on the cosmological constant problem", *hep-th/1502.05296*.
- [42] Linder, E.V. "Quintessence's last stand?", *Phys. Rev. D* **91** (2015), 063006.
- [43] Chiba, T., Okabe, T. & Yamaguchi, M. "Kinetically driven quintessence", *Phys. Rev. D* **62** (2000), 023511.
- [44] Armendariz-Picon, C., Mukhanov, V. & Steinhardt, P.J. "Dynamical solution to the problem of a small cosmological constant and late-time cosmic acceleration", *Phys. Rev. Lett.* **85** (2000), 4438.
- [45] Saridakis, E.N. & Ward, J. "Quintessence and phantom dark energy from ghost D-branes", *Phys. Rev. D* **80** (2009), 083003.
- [46] Sheykhi, A. & Bagheri, A. "Quintessence ghost dark energy model", *Europhys. Lett.* **95** (2011), 39001.
- [47] Böhmer, C.G., Tamanini, N. & Wright, M. "Interacting quintessence from a variational approach. II. Derivative couplings", *Phys. Rev. D* **91** (2015), 123003.
- [48] Li, D. & Scherrer, R.J. "Classifying the behavior of noncanonical quintessence", *Phys. Rev. D* **92** (2015), 083509.
- [49] Kamenshchik, A., Moschella, U., & Pasquier, V. "An alternative to quintessence", *Phys. Lett. B* **511** (2001), 265.
- [50] Fabris, J.C., Goncalves, S.V.B., & de Souza, P.E. "Density perturbations in a universe dominated by the Chaplygin gas", *Gen. Rel. Grav.* **34** (2002), 53.
- [51] Bento, M.C., Bertolami, O., & Sen, A.A. "Generalized Chaplygin gas, accelerated expansion and dark energy-matter unification", *Phys. Rev. D* **66** (2002), 043507.
- [52] Avelino, P.P., Beilja, L.M.G., de Carvalho, J.P.M., Martins, C.J.A.P. & Pinto, P. "Alternatives to quintessence model building", *Phys. Rev. D* **67** (2003), 023511.
- [53] Bean, R., & Dore, O. "Are Chaplygin gases serious contenders for the dark energy?", *Phys. Rev. D* **68** (2003), 023515.
- [54] Sandvik, S.B., Tegmark, M., Zaldarriaga, M., & Waga, I. "The end of unified dark matter?" *Phys. Rev. D* **69** (2004), 123524.
- [55] Dindam, B.R., Kumar, S., & Sen, A.A. "Inflationary generalized Chaplygin gas and dark energy in the light of the Planck and BICEP2 experiments", *Phys. Rev. D* **90** (2014), 083515.

- [56] Ebadi, H., & Moradpour, H. "Thermodynamical description of modified generalized Chaplygin gas model of dark energy", *Int. J. Theor. Phys.* **55** (2016), 1612.
- [57] Fabris, J.C., Goncalves, S.V.B., Velten, H.E.S., & Zimdahl, W. "Matter power spectrum for the generalized Chaplygin gas model: The newtonian approach", *Phys. Rev. D* **78** (2008), 103523.
- [58] Eiroa, E.F. "Thin-shell wormholes with a generalized Chaplygin gas", *Phys. Rev. D* **80** (2009), 044033.
- [59] Bejarano, C., & Eiroa, E.F. "Dilaton thin-shell wormholes supported by a generalized Chaplygin gas", *Phys. Rev. D* **84** (2011), 064043.
- [60] Kuhfittig, P.K.F. "Wormholes admitting conformal Killing vectors and supported by generalized Chaplygin gas", *Eur. Phys. J. C* **75** (2015), 357.
- [61] Nojiri, S. & Odintsov, S.D. "Introduction to modified gravity and gravitational alternative for dark energy", *Int. J. Geom. Meth. Mod. Phys.* **04** (2007), 115.
- [62] De Felice, A. & Tsujikawa, S. " $f(R)$ theories", *Living Rev. Rel.* **13** (2010), 3.
- [63] Sotiriou, T.P. & Faraoni, V. " $f(R)$ theories of gravity", *Rev. Mod. Phys.* **82** (2010), 451.
- [64] Ziaie, A.H., Atazadeh, K., & Rasouli, S.M.M. "Naked Singularity Formation In $f(R)$ Gravity", *Gen. Rel. Grav.* **43** (2011), 2943.
- [65] Jennings, E., Baugh, C.M., Li, B., Zhao, G.-B. & Koyama, K. "Redshift-space distortions in $f(R)$ gravity", *Mon. Not. R. Astron. Soc.* **425**, (2012), 2128.
- [66] Carloni, S., Goswami, R. & Dunsby, P.K.S. "A new approach to reconstruction methods in $f(R)$ gravity", *Class. Quantum Grav.* **29**, (2012), 135012.
- [67] Aviles, A., Bravetti, A., Capozziello, S. & Luongo, O. "Updated constraints on $f(R)$ gravity from cosmography", *Phys. Rev. D* **87** (2013), 044012.
- [68] Makarenko, Andrey N., Odintsov, S. & Olmo, Gonzalo J. "Born-Infeld $f(R)$ gravity", *Phys. Rev. D* **90** (2014), 024066.
- [69] Cataneo, M., *et al.* "New constraints on $f(R)$ gravity from clusters of galaxies", *Phys. Rev. D* **92** (2015), 044009.
- [70] Battye, R.A., Bolliet, B. & Pearson, J.A. " $f(R)$ gravity as a dark energy fluid", *Phys. Rev. D* **93** (2016), 044026.
- [71] Bertolami, O., Böhmer, C.G., Harko, T. & Lobo, F.S.N. "Extra force in $f(R)$ modified theories of gravity", *Phys. Rev. D* **75** (2007), 104016.

- [72] Bertolami, O. & Páramos, J. “Do $f(R)$ theories matter?”, *Phys. Rev. D* **77** (2008), 084018.
- [73] Bertolami, O., Lobo, F.S.N., & Páramos, J. “Nonminimal coupling of perfect fluids to curvature”, *Phys. Rev. D* **78** (2008), 064036.
- [74] Harko, T. “Modified gravity with arbitrary coupling between matter and geometry”, *Phys. Lett. B* **669** (2008), 376.
- [75] Nesseris, S. “Matter density perturbations in modified gravity models with arbitrary coupling between matter and geometry”, *Phys. Rev. D* **79** (2009), 044015.
- [76] Harko, T. & Lobo, F.S.N. “ $f(R, L_m)$ gravity”, *Eur. Phys. J. C* **70** (2010), 373.
- [77] Harko, T, Lobo, Francisco S.N., Nojiri, S. & Odintsov, Sergei D. “ $f(R, T)$ gravity”, *Phys. Rev. D* **84** (2011), 024020.
- [78] Houndjo, M.J.S., Alvarenga, F.G., Rodrigues, M.E., Jardim, D.F. & Myrzakulov, R. “Thermodynamics in little rip cosmology in the framework of a type of $f(R, T)$ gravity”, *gr-qc/1207.1646*.
- [79] Sharif, M. & Zubair, M. “Thermodynamics in $f(R, T)$ theory of gravity”, *J. Cosmol. Astropart. Phys.* **03** (2012), 028.
- [80] Jamil, M., Momeni, D. & Ratbay, M. “Violation of the first law of thermodynamics in $f(R, T)$ gravity”, *Chin. Phys. Lett.* **29** (2012), 109801.
- [81] Sharif, M. & Zubair, M. “Thermodynamic behavior of particular $f(R, T)$ -gravity models”, *J. Exp. Theor. Phys.* **117** (2013), 248.
- [82] Alvarenga, F.G., Houndjo, M.J.S., Monwanou, A.V. & Chabi Orou, J.B. “Testing some $f(R, T)$ gravity models from energy conditions”, *J. Mod. Phys.* **04** (2013), 130.
- [83] Shabani, H. & Farhoudi, M. “ $f(R, T)$ cosmological models in phase-space”, *Phys. Rev. D* **88** (2013), 044048.
- [84] Sharif, M. & Zubair, M. “Energy conditions in $f(R, T, R_{\mu\nu}T^{\mu\nu})$ gravity”, *J. High Energy Phys.* **12** (2013), 079.
- [85] Kiani, F. & Nozari, K. “Energy conditions in $F(T, \Theta)$ gravity and compatibility with a stable de Sitter solution”, *Phys. Lett. B* **728** (2014), 554
- [86] Shabani, H. & Farhoudi, M. “cosmological and solar system consequences of $f(R, T)$ gravity models”, *Phys. Rev. D* **90** (2014), 044031.
- [87] Noureen, I. & Zubair, M. “Dynamical instability and expansion-free condition in $f(R, T)$ gravity”, *Eur. Phys. J. C* **75** (2015), 62.

- [88] Azizi, T. & Yaraie, E. "Gödel-type universes in Palatini $f(R)$ gravity with a non-minimal curvature-matter coupling", *Int. J. Theor. Phys.* **55** (2016), 176.
- [89] Joshi; Barrientos, O. & Rubilar, Guillermo F. "Surface curvature singularities of polytropic spheres in Palatini $f(R, T)$ gravity", *Phys. Rev. D* **93** (2016), 024021.
- [90] Alves, M.E.S., Moraes, P.H.R.S., de Araujo, J.C.N. & Malheiro, M. "Gravitational waves in the $f(R, T)$ theory of gravity", *gr-qc/1604.03874*.
- [91] Shabani, H. & Ziaie, A.H. "Stability of the Einstein static universe in $f(R, T)$ gravity", *gr-qc/1606.07959*.
- [92] Riess, A.G., *et al.* "Type Ia supernova discoveries at $z > 1$ from the Hubble Space Telescope: evidence for past deceleration and constraints on dark energy evolution", *Astrphys. J.* **607** (2004), 665.
- [93] Astier, P., *et al.* "The Supernova Legacy Survey: measurement of Ω_M , Ω_Λ and w from the first year data set", *A&A* **447** (2006), 31.
- [94] Rapetti, D., *et al.* "A kinematical approach to dark energy studies", *Mon. Not. R. Astron. Soc.* **375**, (2007), 1510.
- [95] Wu, P. & Yu, H. "Constraints on the unified dark energy; dark matter model from latest observational data", *J. Cosmol. Astropart. Phys.*, **03** (2007), 015
- [96] Bento, M.C., Bertolami, O., & Sen, A.A. "Generalized Chaplygin gas and cosmic microwave background radiation constraints", *Phys. Rev. D* **67** (2003), 063003.
- [97] Zhu, Z.-H. "Generalized Chaplygin gas as a unified scenario of dark matter/energy: Observational constraints", *A&A* **423** (2004), 421.
- [98] Wu, P., & Yu, H. "Generalized Chaplygin gas model: Constraints from Hubble parameter versus redshift data", *Phys. Lett. B*, **644** (2007), 16.
- [99] Wu, P., & Yu, H. "Interacting generalized Chaplygin gas", *Class. Quantum Grav.*, **24** (2007), 4661.
- [100] Amendola, L., Waga I. & Finelli, F., "Observational constraints on silent quartessence", *J. Cosmol. Astropart. Phys.*, **11** (2005), 009.
- [101] Elmardi, M., Abebe, A. & Tekola, A. "Chaplygin-gas Solutions of $f(R)$ Gravity", *gr-qc/1603.05535*.
- [102] Borowiec, A., Stachowski, A., Szydlowski, M. & Wojnar, A. "Inflationary cosmology with Chaplygin gas in Palatini formalism", *J. Cosmol. Astropart. Phys.*, **01** (2016), 040.

- [103] Sandvik, Håvard B., Tegmark, M., Zaldarriaga, M. & Waga, I. "The end of unified dark matter?", *Phys. Rev. D* **69** (2004), 123524.
- [104] Popolo, A. Del, *et al.* "Shear and rotation in Chaplygin cosmology", *Phys. Rev. D* **87** (2013), 043527.
- [105] Sahni, V., Saini, T.D., Starobinsky, A.A., & Alam, U. "Statefinder—a new geometrical diagnostic of dark energy", *JETP Lett.* **77** (2003), 201.
- [106] Alam, U., Sahni, V., Saini, T.D. & Starobinsky, A.A. "Exploring the expanding Universe and dark energy using the statefinder diagnostic", *Mon. Not. R. Astron. Soc.* **344**, (2003), 1057.
- [107] Zimdahl, W. & Pavon, D. "Letter: statefinder parameters for interacting dark energy", *Gen. Rel. Grav.* **36** (2004), 1483.
- [108] Zhang, X. "Dark energy constraints from the cosmic age and supernova", *Phys. Lett. B*, **611** (2005), 1.
- [109] Zhang, X. "Statefinder diagnostic for holographic dark energy model", *Int. J. Mod. Phys. D*, **14** (2005), 1597.
- [110] Zhang, J., Zhang, X. & Liu, H. "Statefinder diagnosis for the interacting model of holographic dark energy", *Phys. Lett. B*, **659** (2008), 26
- [111] Setare, M.R., Zhang, J. & Zhang, X. "Statefinder diagnosis in a non-flat universe and the holographic model of dark energy", *J. Cosmol. Astropart. Phys.*, **0703** (2007), 007.
- [112] Chang, B.R., Liu, H.Y., Xu, L.X., Zhang, C.W. & Ping, Y.L. "Statefinder parameters for interacting phantom energy with dark matter", *J. Cosmol. Astropart. Phys.*, **0701** (2007), 016.
- [113] Shao, Y. & Gui, Y. "Statefinder parameters for tachyon dark energy model", *Mod. Phys. Lett. A*, **23** (2008), 65.
- [114] Malekjani, M., Khodam-Mohammadi, A. & Nazari-Pooya, N. "Generalized Chaplygin gas model: cosmological consequences and statefinder diagnosis", *Astrophys. Space Sci.*, **334** (2011), 193.
- [115] Zhang, L., Cui, J., Zhang, J., Zhang, X. "Interacting model of new agegraphic dark energy: cosmological evolution and statefinder diagnostic", *Int. J. Mod. Phys. D*, **19** (2010), 21.
- [116] Khodam-Mohammadi, A. & Malekjani, M. "Cosmic behavior, statefinder diagnostic and $w - w'$ analysis for interacting new agegraphic dark energy model in non-flat universe", *Astrophys. Space Sci.*, **331** (2010), 265.
- [117] Haghani, Z., Harko, T., Lobo, F.S.N., Sepangi, H.R. & Shahidi, S. "Further matters in space-time geometry: $f(R, T, R_{\mu\nu}T^{\mu\nu})$ gravity", *Phys. Rev. D* **88** (2013), 044023.

- [118] Sharif, M. & Zubair, M. "Cosmological reconstruction and stability in $f(R, T)$ gravity", *Gen. Rel. Grav.* **46** (2014), 1723.
- [119] Capozziello, S. & Faraoni, V., *Beyond Einstein Gravity*, (Springer, Netherlands, 2011).
- [120] Pradhan, A., Ahmed, N. & Saha, B. "Reconstruction of modified $f(R, T)$ with $\Lambda(T)$ gravity in general class of Bianchi cosmological models", *Can. J. Phys.*, **93** (2015), 654.
- [121] Saho, P.K. & Sivakumar, M. "LRS Bianchi type-I cosmological model in $f(R, T)$ theory of gravity with $\Lambda(T)$ ", *Astrophys. Space Sci.*, **357** (2015), 60.
- [122] Poplawski, Nikodem J. "A Lagrangian description of interacting dark energy", *gr-qc/0608031*.
- [123] Bertolami, O., Gil Pedro, F. & Le Delliou, M. "Dark energy–dark matter interaction and putative violation of the equivalence principle from the Abell cluster A586", *Phys. Lett. B* **654** (2007), 165.
- [124] Amanullah, R., *et al.* "Spectra and Hubble space telescope light curves of six type Ia supernovae at $0.511 < z < 1.12$ and the Union2 compilation", *Astrophys. J.* **716** (2010), 712.
- [125] Farooq, O., *et al.* "Hubble parameter measurement constraints on the redshift of the deceleration-acceleration transition, dynamical dark energy, and space curvature", *astro-ph/1607.03537*.
- [126] Simon, J., Verde, L., & Jimenez, R. "Constraints on the redshift dependence of the dark energy potential", *Phys. Rev. D* **71** (2005), 123001.
- [127] Stern, D., *et al.* "Cosmic chronometers: Constraining the equation of state of dark energy. II. a spectroscopic catalog of red galaxies in galaxy clusters", *Astrophys. J.* **188** (2010), 280.
- [128] Moresco, M., *et al.* "Improved constraints on the expansion rate of the Universe up to z 1.1 from the spectroscopic evolution of cosmic chronometers", *J. Cosmol. Astropart. Phys.*, **08** (2012), 006.
- [129] Blake, C., *et al.* "The WiggleZ Dark Energy Survey: Joint measurements of the expansion and growth history at $z < 1$ ", *Mon. Not. R. Astron. Soc.* **425**, (2012), 405.
- [130] Font-Ribera, A., *et al.* "Quasar-Lyman α forest cross-correlation from BOSS DR11: Baryon acoustic oscillations", *J. Cosmol. Astropart. Phys.*, **05** (2014), 027.
- [131] Delubac, T., *et al.* "Baryon acoustic oscillations in the Ly α forest of BOSS DR11 quasars", *A&A* **574** (2015), A59.

- [132] Moresco, M., *et al.* "A 6% measurement of the Hubble parameter at $z \sim 0.45$: direct evidence of the epoch of cosmic re-acceleration", *J. Cosmol. Astropart. Phys.*, **05** (2016), 014
- [133] Cuesta, J.A., *et al.* "The clustering of galaxies in the SDSS-III Baryon Oscillation Spectroscopic Survey: Baryon acoustic oscillations in the correlation function of LOWZ and CMASS galaxies in Data Release 12", *Mon. Not. R. Astron. Soc.* **457**, (2016), 1770.
- [134] <https://github.com/CosmologyTaskForce/CoChiSquare/tree/alpha>;
DOI:10.5281/zenodo.13197, (2014).
- [135] <http://www.wolfram.com/>
- [136] <https://www.python.org/psf/>
- [137] Perivolaropoulos, L. & Nesseris, S., <http://leandros.physics.uoi.gr/cosmofit.htm>.